Sedimentologika

Research article

Micro-facies characterization of the Cane Creek Shale, Paradox Basin, Utah: implications of diagenetic controls on reservoir quality

Raul I. Ochoa[1*], Lauren P. Birgenheier[1], Elliot Jagniecki[2], Michael D. Vanden Berg[2]

[1] Department of Geology and Geophysics, University of Utah, 115 S 1460 E, Salt Lake City, UT, 84112, USA
[2] Utah Geological Survey, PO Box 146100, Salt Lake City, UT 84114, USA

*corresponding author: Raul Ochoa (riochoa88@gmail.com)

doi: 10.57035/journals/sdk.2024.e22.1278

Editors: Carolina Keim and Or Bialik
Reviewers: Two anonymous reviewers
Copyediting, layout and production: Romain Vaucher, Farid Saleh and Gabriel Bertolini

Submitted: 09.10.2023
Accepted: 30.07.2024
Published: 18.10.2024

Abstract | The fine-grained Pennsylvanian Cane Creek Shale of the Paradox Formation, Paradox Basin, Utah exhibits relatively thin cyclic interbeds of contrasting lithologies including fine sandstone to siltstone, organic-rich carbonate and dolomitic mudstone, and evaporites. As such, it provides a unique opportunity to evaluate micro-facies and the fluid storage capacity potential of mixed fine-grained systems. Micro-facies descriptions were performed using core and petrographic analyses, including scanning electron microscopy with energy dispersive spectroscopy. The study leverages core-based porosity and permeability data, as well as previous core description. These data are used together to explore mineralogical depositional and diagenetic controls on porosity and permeability. Twelve micro-facies were described based on sedimentological textures, grain size, lithology, and mineralogy categorized into three groups: 1) sandstone to siltstone, 2) mudstone, and 3) evaporitic micro-facies. Sandstone to siltstone micro-facies exhibit variable porosity and permeability. Porosity connectivity is dependent on the degree of authigenic cementation and compaction that negatively impacts porosity. Mudstone micro-facies show less variability in porosity and permeability; and are characterized by carbonate content, organic-matter, and clay nanopores. The development of early carbonate grains maintains porosity in mudstone and dolomitic siltstone micro-facies. Evaporitic micro-facies represented by evaporitic sabkha-like conditions are characterized by pore-reducing anhydrite and halite cement. A diagenetic paragenetic sequence was developed to assess the timing and impact of mineralogy on reservoir quality. Early (eogenetic), Middle (mesogenetic), and Late (telogenetic) stages correspond with diagenetic stages and known tectonic basin events. Syndepositional dolomite and diagenetic illite/smectite authigenic cements are the main controls on reservoir quality and have opposing effects related to porosity and permeability by preserving early pore space or reducing porosity and permeability.

Lay summary | The authors present a high-resolution, micro-scale study of an alternating fine-grained siliciclastic and dolomitic mudstone interval of the Pennsylvanian Cane Creek Shale of the Paradox Basin in the Paradox Basin, Utah. This study uses scanning electron microscopy and elemental dispersive spectroscopy (EDS) with measured porosity and permeability to identify twelve micro-facies for the Cane Creek Shale. A diagenetic sequence is constructed from observations to address how detrital and diagenetic mineralogy affect porosity and permeability trends. Porosity and permeability trends with described micro-facies and diagenetic mineralogy can be used to identify optimal intervals for hydrocarbon exploration.

Keywords: Mudstone sedimentology, Mudrocks, Reservoir characterization, Petrographic analysis, Diagenesis

1. Introduction

Characterizing and quantifying matrix porosity and permeability in fine-grained deposits (i.e., mudstones and fine-grained sandstones) is critical in developing energy applications such as unconventional hydrocarbon resources, geothermal resources, hydrogen storage, and carbon capture and storage. A focus on fine-grained deposits and mudstones is led by enhanced technologies commonly applied to hydrocarbon development, specifically horizontal drilling and hydraulic stimulation (Sondergeld et al., 2010). Hydraulic stimulation along with petrologic mineral analyses have also been applied to geothermal development for energy applications (Lutz et al., 2010). In addition, fine-grained evaporitic deposits can serve as potential seals and reservoirs for hydrogen and carbon dioxide storage due to their low porosity and permeability.

Petrographic analyses in literature have highlighted the importance of fine-grained sedimentary rocks by better understanding these sedimentary facies towards energy applications including shale-gas development, geothermal exploration, and lithium brine extraction (e.g., Taylor & Macquaker, 2014; Li & Schieber, 2020). Fine-grained deposits from detrital quartz-rich, very fine sandstone to siliceous mudstone lithologies host a myriad of complex heterogeneities at the meso to micro-scale (Milliken & Olson, 2017; Egenhoff et al., 2019). Meso-scale variability here refers to observations from core and micro-scale variability observed in fine-grained deposits <62.5 μm (Blair & McPherson, 1999). Loucks et al. (2012) defined pore scales to include micropores (<62.5 μm) between clay and cements domains, and organic matter pores as nanopores (<1 μm). This includes variability in lithology and mineralogy, in addition to chemical and physical diagenetic changes, all of which affect reservoir quality (Quandt et al., 2022), specifically the development of porosity and permeability. Therefore, it is key to understand the micro-scale heterogeneities from petrography that characterize fine-grained formation. Understanding the temporal pore-scale diagenetic development and matrix heterogeneities in fine-grained deposits is important to assess fluid storage capacity (e.g., hydrocarbon, CO_2, hydrogen, water) in terms of reservoir quality and seal performance.

This contribution is focused on one particular fine-grained, mudstone-dominated succession, the Cane Creek Shale of the Paradox Basin, Utah, but lends to the growing number of micro-scale analyses and authigenic cement studies applied towards understanding reservoir quality for energy development (Howard, 1992; Jagniecki et al., 2019; Busch et al., 2022; Quandt et al., 2022; McCormack et al., 2023). As compared to many fine-grained depositional systems, the Cane Creek Shale is particularly unique in its wide range of fine-grained lithologies that include cyclically interbedded carbonate to dolomitic organic-rich mudstone, sandstone and siltstone, and evaporites. The results could pertain to similarly lithologically or mineralogically diverse, cyclically interbedded fine-grained successions worldwide. The facies and stratigraphic motif are particularly common in Late Paleozoic cyclothems worldwide that were deposited in response to rapid and frequent cyclical icehouse-driven eustatic changes (Fielding, 2021).

The goals of this study are to use high-resolution petrography to 1) address how micro-scale mineralogical heterogeneities (i.e., mineralogical composition and rock fabrics) including authigenic cements that nucleate on detrital grains and pore throats affect porosity and permeability; 2) identify diagenetic processes in pore fluids that impact reservoir quality in cyclically interbedded fine-grained siliciclastic sandstone and siltstone, dolomitic mudstone, and evaporitic successions 3) integrate observations and data with existing studies on burial history modeling to develop a diagenetic paragenetic sequence of events that control the evolution of porosity and permeability in micro-facies to identify potential risks associated with hydrocarbon development. The Cane Creek Shale is estimated to exceed 215 million barrels of oil and 4,530 billion cubic feet of gas with only 5% of the total resource being developed (Whidden et al., 2012; McCormack et al., 2023). In this study, we developed a diagenetic paragenetic sequence to illustrate how mineralogical composition, stages of compaction and authigenic cementation, and basin history help identify potential risks associated with hydrocarbon development. Diagenetic processes influence the overall hydrocarbon storage capacity (porosity) and producibility (permeability) of the Cane Creek Shale.

1.1. Geologic background

The present-day Paradox Basin is a northwest-southeast trending asymmetric flexural basin spanning southeastern Utah, southwestern Colorado, and portions of Arizona and New Mexico (Figure 1) (Barbeau, 2003; Trudgill, 2011). The Paradox Basin developed as a depression adjacent to crustal loading related to the Uncompahgre Uplift, a paleotopographic high formed due to collision between Gondwana and Laurentia. Regional uplift was initiated in the Late Mississippian and Early Pennsylvanian and formed the formation of the Ancestral Rocky Mountains during the Middle Pennsylvanian through the Permian (Stokes, 1986; Barbeau, 2003; Whidden et al., 2014). The Paradox Basin was one of many paleotopographic depressions associated with neighboring paleotopographic highs (i.e., the Ancestral Rocky Mountains) that developed during this time.

1.2. Stratigraphy

The fine-grained deposits of the Middle Pennsylvanian Cane Creek Shale, within the Hermosa Group in the Paradox Basin, are found within the broader Paleozoic stratigraphy (Figure 2). The greater Hermosa Group records clastic-evaporitic deposition during the Middle Pennsylvanian (Hite, 1960; Hite et al., 1984). Within the Hermosa Group, the Paradox Formation contains multiple

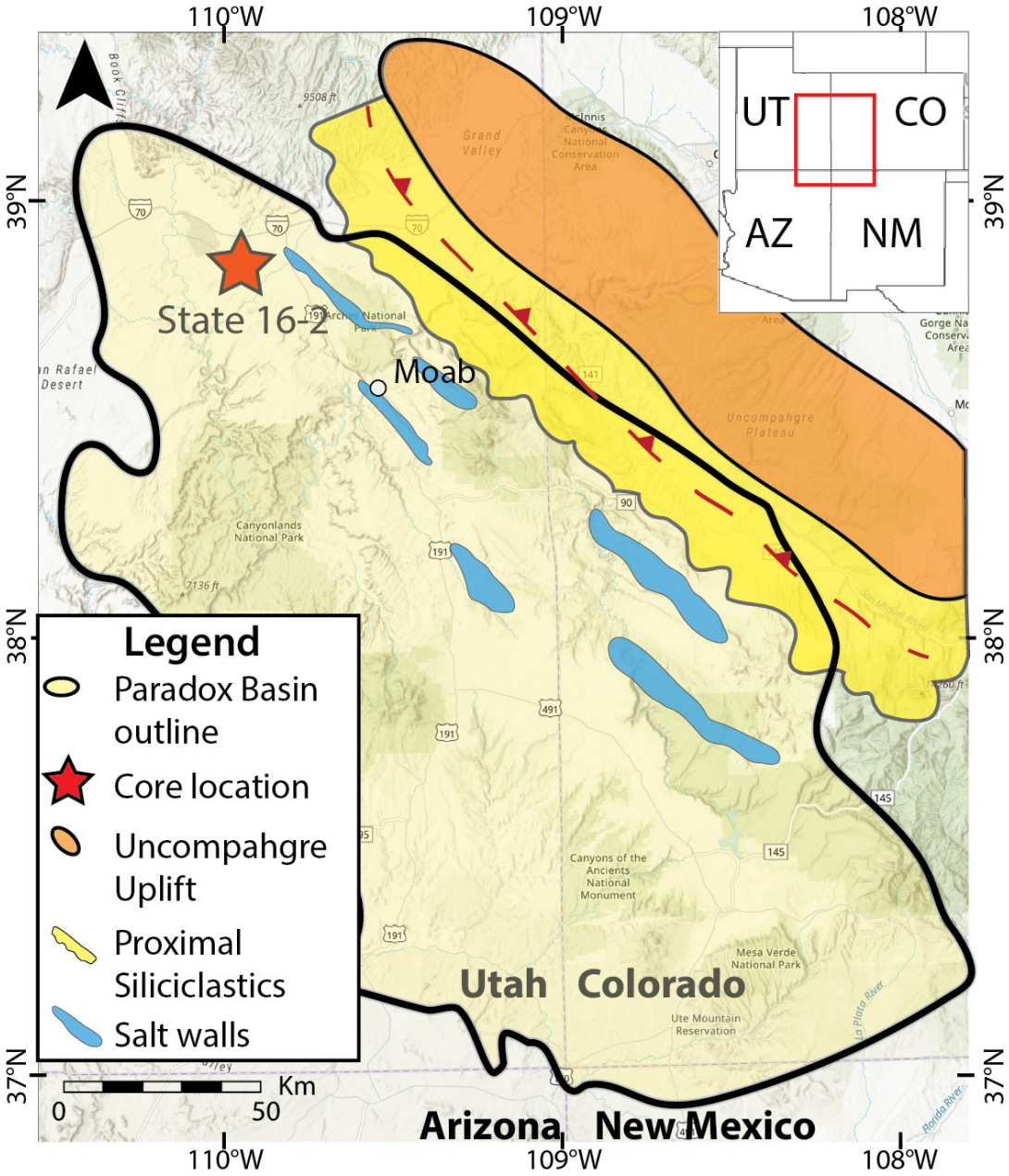

Figure 1 | Paradox Basin outline. Red star indicates Zephyr Energy State 16-2 research core location in southeastern Utah (northern Paradox Basin), USA.

dolomitic, organic-rich shales that are known as hydrocarbon source rock intervals, including the Cane Creek Shale, Chimney Rock, Gothic, and Hovenweep units (Figure 2) (Whidden et al., 2014). Cane Creek Shale fine-grained rocks were deposited during restricted sea waters in a sabkha environment leading to siliciclastic, carbonate, organic-rich, and evaporitic facies (Jagniecki et al., 2019). Restriction was controlled by periodic flooding of narrow seaways from the open sea to the northwest and southeast (Hite, 1960; Goldhammer et al., 1991). The clastic-evaporitic cycles were deposited in a tidally-influenced epeiric sea that experienced seaway restriction from time to time (Hite, 1960; Hite & Buckner, 1981; Jagniecki et al., 2019). Hite (1960) described "saline-facies" that represent sabkha-type systems (Jagniecki et al., 2019) that grade laterally basinward into limestone facies.

During the early to middle Paleozoic (Cambrian to Mississippian) prior to basin development, the majority of this region was a stable craton with deposition of mainly shallow-marine carbonates (Nuccio & Condon, 1996; Whidden et al., 2014). Within the Paradox Basin, the oldest deposited sediments include Cambrian clastics, including the Tapeats Sandstone and the Bright Angel shale, unconformably overlying igneous and metamorphic basement rocks (Figure 2) (Nuccio & Condon, 1996; Katherine et al., 2014). Devonian clastics unconformably overlie the Cambrian sedimentary rocks that include sandstones and shales. Devonian to Mississippian carbonates, related to a regional marine transgression, unconformably overlie Devonian clastics. Exposure and karsting of limestones deposits occurred during uplift in the Late Mississippian (Whidden et al., 2014).

From the Middle to Upper Pennsylvanian, alternating episodic events of marine and evaporitic conditions in the Paradox Basin were recorded as cyclic deposits of clastics, limestones, organic-rich shales, and evaporites (Hite,

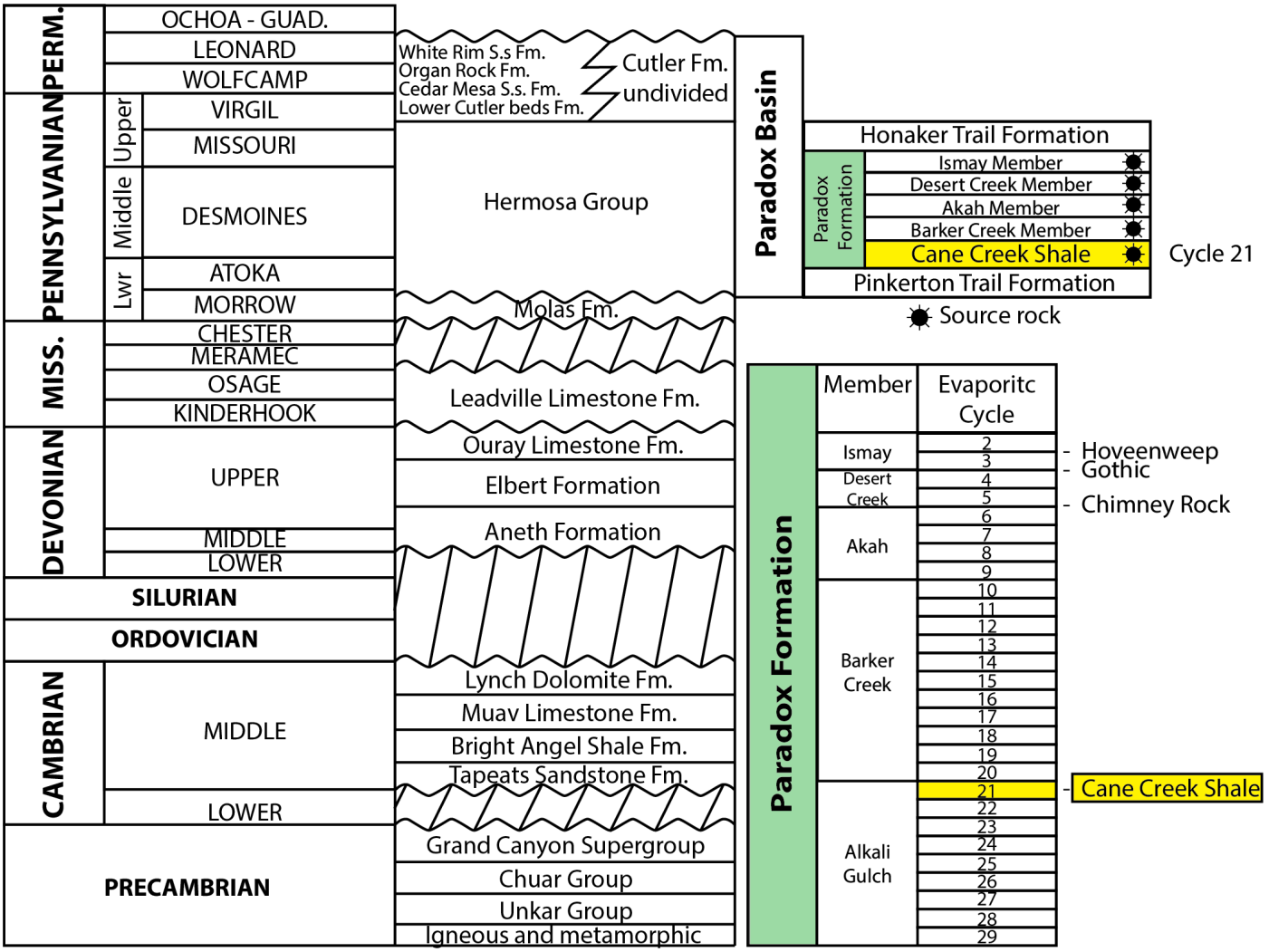

Figure 2 | Paleozoic stratigraphic column. Source rock units of the Paradox Formation including the Cane Creek Shale. The Cane Creek Shale is part of Cycle 29 originally described by Hite (1960). North American geologic time scale modified from Soreghan et al. (2009), Stevenson & Wray (2009), and Whidden et al. (2013). Perm. = Permian, Miss. = Mississippian, Lwr = Lower, S.s. = Sandstone, Fm. = Formation.

1960). Within the Middle Pennsylvanian package of the Paradox Basin, 29 evaporitic and clastic cycles were identified and named by Hite (1960) and 80 cycles were later described (Rasmussen & Rasmussen, 2009; Whidden et al., 2014). These cycles have been interpreted to represent lowstand and highstand glacio-eustatic sea-level fluctuations respectively (Goldhammer et al., 1991; Rasmussen & Rasmussen, 2009; Whidden et al., 2014).

2. Dataset and previous work

Characterization of the Cane Creek Shale is based on an approximately 30-meter cored interval of Zephyr Energy State 16-2 well from southeastern Utah near Moab, UT (Figure 1). The State 16-2 core is measured in feet but is reported herein as meters (m) and feet (′). Total cored Cane Creek Shale is from 2,938 m (9,638′) to 2,968 m (9,728′) (27 m or 90′ total) with 2,965 m (9,728′) to 2,971 m (9,748′) (6 m or 20′ total) of Salt 22, Clastic 23, and Salt 23 of the Alkali Gulch (Lower Paradox Formation) (Figure 3) (Jagniecki et al., 2019; McCormack et al., 2023). Zephyr Energy State 16-2 research well was collected from the existing State 16-42 well pad on Utah School and Institutional Trust Lands Administration (SITLA) land in the Gunnison Valley Unit, northern Paradox Basin.

Core facies were previously documented in Zephyr Energy State 16-2 core based on visual grain size, sedimentary structures, and mineralogical X-ray Diffraction (XRD) also shown in the log (Figure 3). Core facies include: 1) anhydritic-dolomudstone; 2) calcareous silty mudstone; 3) coarse crystalline halite; 4) debris flow; 5) fine-grained, sandy siltstone; 6) organic-rich mudstone; 7) silty-dolomitic mudstone (Figure 3) (McCormack et al., 2023).

3. Methods

From the 27 m (90′) cored interval of Cane Creek Shale from Zephyr Energy State 16-2, 79 plugs were collected. Completely fractured samples (n=18) were not used for porosity and permeability measurements. Intact whole core plugs were used to measure porosity and permeability data using conventional core analysis at Stratum Reservoir, LLC. These data were collected for 62 out of the 80 samples. Rock samples were cleaned using the Dean-Stark-distillation-extraction method (Dean & Stark, 1920). Porosity measurements were collected at ambient

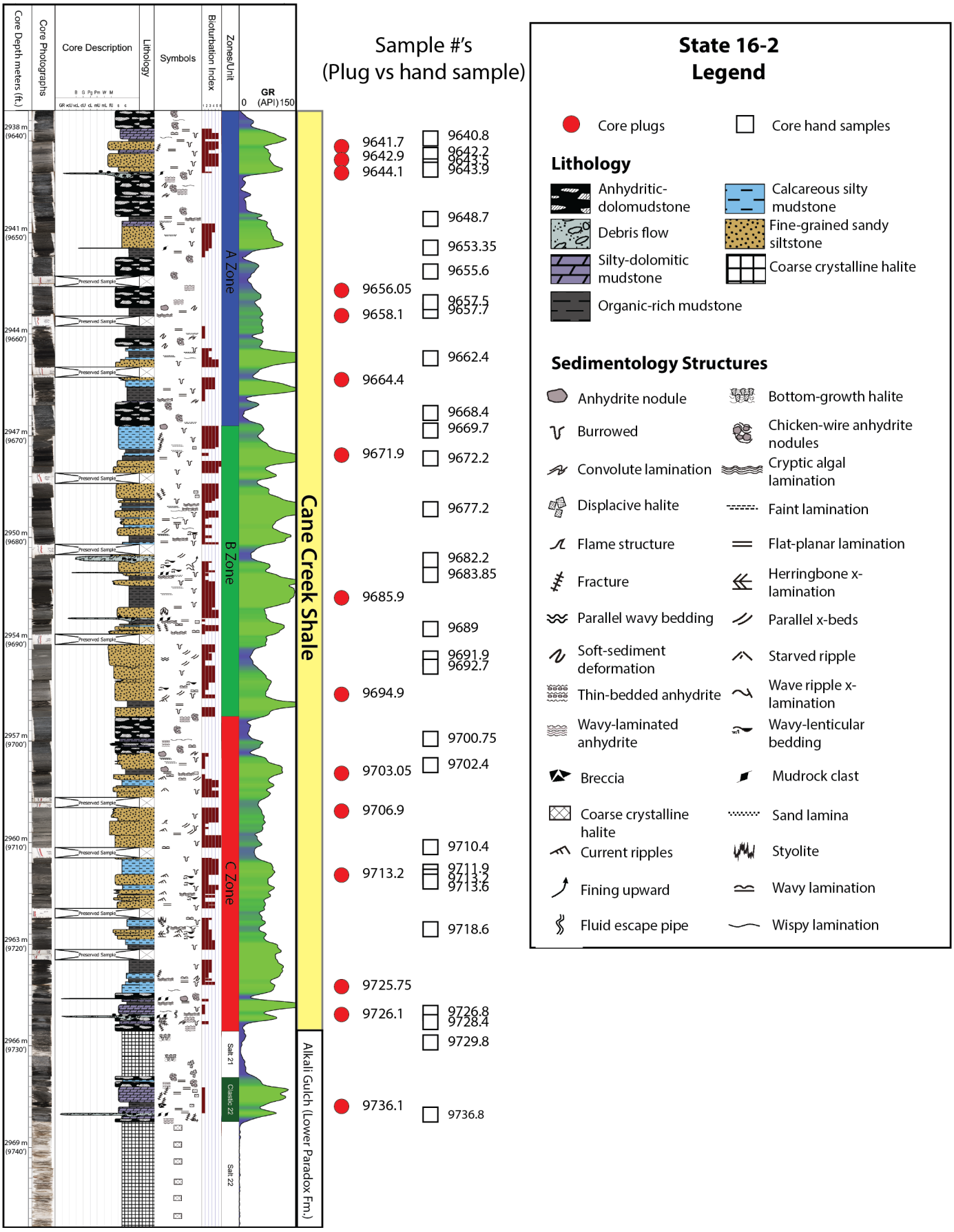

Figure 3 | Zephyr Energy State 16-2 well previous core log (McCormack et al., 2023), with added plug and hand sample depths from this study. Core description for an approximately 30 m (98') interval. Zephyr Energy State 16-2 research core (McCormack et al., 2023) was used as the basis for this study with added core plugs and core hand sampling for petrography, SEM, and measured porosity and permeability analysis.

pressure and a net confining stress of 600 psi. Permeability measurements were collected at ambient pressure and corrected for Klinkenberg gas slippage. Ultra-thin (15-20 µm) thin sections (n=16) from the eighty plugs from the core were prepared for thin section analysis (Figure 3). An additional 19 large format and 4 standard, ultra-thin (15-20

μm) thin sections were selected and prepared from whole core sampling (n=29). The thin sample set (n=45 total) included 20 sandstone, 4 siltstone, 14 mudstone, and 7 evaporitic thin sections. Samples were impregnated with a blue epoxy under vacuum to highlight effective pore space in thin sections. A Nikon ECLIPSE Microscope and INFINITY ANALYZE software was used to examine thin sections petrographically and collect images.

Backscattered-Electron Detector (BSED) imaging scanning electron microscopy (SEM) in conjunction with energy dispersive spectroscopy (EDS) was used to analyze composite elemental maps along with traditional petrography imaged thin sections. BSEM and EDS were used for high-resolution imaging and characterization of mineralogical descriptors, pore types, and micro-facies. Micro-facies were expanded upon from existing core lithological macro-facies descriptions (Jagniecki et al., 2019; McCormack et al., 2023). Traditional petrographic and SEM analysis was used to describe grain size and composition, cements, matrix, mineralogy, lithology, sedimentary features, and textures. Petrographic descriptors and naming schemes for sandstone and mudstone micro-facies were modified from Dunham (1962) and Lazar et al. (2015). Pore types are described following Loucks et al. (2012) originally modified from Choquette & Pray (1970). Pore types described include intergranular or intercrystalline, intragranular, fracture porosity, or organic matter porosity (Choquette & Pray, 1970; Lucia, 1983; Loucks et al., 2012).

SEM with EDS analysis was performed on the FEI Quanta 600 FEG at the Biotechnology Nanofab lab at the University of Utah, Salt Lake City, UT. Thin sections were coated with a 20 nm thick layer of carbon. Carbon coating is used to increase conductivity, leading to a decrease in charging by electrons. All backscatter images were captured using either a 15 or 20 kV acceleration voltage, spot size of 4 or 5, and working distances between 10 and 14 mm. Composite elemental mineral maps from EDS were generated and analyzed using APEX software.

4. Results

4.1. Micro-facies

Twelve micro-facies are described here in detail based on petrographic and SEM descriptions, grain size, texture and fabric, pore types, authigenic cements, and mineralogical composition from SEM-EDS composite elemental maps (Tables 1 and 2). Micro-facies scale of observation relates specifically to nano-to-micro scale (i.e., thin section) heterogeneities that have implications on reservoir quality specific to porosity and permeability along with core scale observations. Detailed micro-facies analyses provide information on mineralogy, sedimentological textures, and grain size changes that can aid with depositional environment implications. Following Loucks et al. (2012), most pores in the Cane Creek Shale are micropores (<62.5 μm) based on scale but described here based on their pore type character (i.e., intergranular, intragranular, fracture porosity, organic matter porosity) unless otherwise noted.

The twelve micro-facies were subdivided based on grain size, mineralogy, and lithological facies grouped into three categories following the Udden-Wentworth grain scale (Udden, 1914): 1) sandstone (63-2000 micron mean grain size), although no grain size >250 was observed, to siltstone (4-63 micron mean grain size), 2) mudstone (<4 micron mean grain size), and 3) evaporitic micro-facies (Tables 1 and 2, Figure 4). Mineralogy was quantified from elemental image analysis under EDS, with elements being reported as percentages, rather than elemental oxide weight percent. Micro-facies were classified based on mineralogy and average grain size following classification from Blair & McPherson (1999) and Udden-Wentworth grain scale. Average grain size was measured from SEM micrographs. Very fine sand to silt-sized grains with less abundant clay-sized grains represent the sandstone to siltstone micro-facies. Clay-sized grains with few silt-sized grains represent the mudstone micro-facies. Anhydrite and halite cements are abundant in the evaporitic micro-facies. SEM with EDS composite elemental maps validated with optical microscope petrography were used to identify micro-facies and interpret mineralogy. Silicon image percent from EDS composite elemental maps can represent detrital and authigenic quartz (silica), feldspar, and clay minerals but is primarily interpreted to assess detrital quartz grains given that the bulk of the silicon is visually identified from petrographic micrographs as detrital quartz grains. Aluminum (Al) and potassium (K) EDS image percentages represent clay domains, cement, and potassium feldspar but are primarily interpreted to assess illite/smectite clay domains and cement as the bulk Al and K is visually identified from micrographs as clays. Calcium and magnesium image percentages represent calcite and dolomite grains and cement. Calcium, sodium, and sulfur image percentages represent calcite, halite, and anhydrite cement.

4.1.1. Sandstone to siltstone micro-facies

Four identified micro-facies represent very fine-grained sandstone to siltstone characterized by mostly siliciclastic composition of detrital quartz and feldspar grains, and illite/smectite matrix and cement. The sandstone to siltstone micro-facies includes (i) calcareous, silty sandstone (n=1), (ii) quartz-rich, very fine sandstone (n=19), (iii) calcareous, dolomitic siltstone (n=2), and (iv) calcareous, halitic siltstone (n=2) micro-facies (Table 1) (Figure 5A–L). Calcareous, silty sandstone and quartz-rich, very fine sandstone micro-facies are made of silt-sized grains of quartz, calcite, and feldspars. From EDS composite elemental maps, quartz-rich, very fine sandstone contains over 45% silicon while calcareous, silty sandstone contains slightly less silicon (34% Si) (Table 1). Calcareous, dolomitic siltstone contains 21% silicon followed by calcareous, halitic siltstone with 10% silicon. The visual abundance of detrital quartz grains also follows the same progression

Micro-facies	Description	Pore types	Authigenic cements	Key components	Sample set	Mineralogy from EDS (%)				Lab Measured	
						Si	Ca	Al+K	Na+Cl	Porosity (%)	Permability (mD)
Calcareous silty mudstone	Fine to medium grained sandstone. Abundant grains of quartz, calcite, dolomite, and feldspars. Some authigenic clays are present in pore space. Feldspars show dissolution.	Intergranular and intragranular pores. Intergranular pores are usually clay-lined or pore-filled. Some uncemented, clean intergranular pores. Secondary, dissolution, intragranular pores present in feldspar grains.	Illite/Smectite as pore-lining and pore-filling cement. Anhydrite as nodule and pore-filling cements. Halite as minor pore-filling cement.	Grains: quartz, feldspar, calcite Cements: illite/smectite, calcite, halite, and pyrite Matrix: N/A	n=1	34%	39%	10%	4%	NA	NA
Fine grained sandy-siltstone	Silt-sized grains of quartz, calcite, and feldspars. Many feldspars show secondary dissolution porosity and some quartz near fractures shows signs of dissolution. Authigenic clays of illite/ smectite are commonly found as pore-lining and pore-filling cements. Halite cement can be present in pores or fractures.	Large intergranular and moderate to large intragranular dissolution porosity. Majority of intergranular pores are clay-lined to clay-filled. Micro porosity from clay-filled pores is present is most intergranular pores. Some fracture porosity is present in some fine-grained sandy siltstone micro-facies samples.	Illite/smectite as pore-lining and pore-filling cements. Pyrite framboids. Some dolomite cement and carbonate present. Halite cement in fractures.	Grains: quartz, feldspar, calcite Cements: illite/smectite, calcite, dolomite, quartz overgrowths, pyrite Matrix: N/A	n=19	>45%	<30%	6-20%	<35%	6.3-11.5% (avg. 8.7%)	0.06 to 0.77 mD (avg .21 mD)
Silty-dolomitic mudstone/ Organic-rich mudstone	Silt-sized grains of quartz, calcite, and feldspars. Feldspars show some minor degree of secondary dissolution. Carbonate and dolomitic cement is present. Authigenic clays of illite and smectite are present as pore-lining and pore-filling cements. Carbonate cement is present as pore cement and fracture fill. Halite and anhydrite present as pore-filling cement.	Primary intergranular porosity with some minor to moderate secondary intragranular dissolution porosity. Majority of primary intergranular pores are clay-lined to clay-filled by authigenic cements. Micro-porosity associated with authigenic cements i present. Fracture porosity in sample appears to be completely cemented.	Illite/smectite is the dominant cement present as pore-lining to pore-filling cements. Additional cements include carbonate cement present in fractures and halite present in intergraular pores.	Grains: quartz, feldspar, dolomite, calcite, Cements: illite/smectite, dolomite, calcite, pyritie Matrix: micrite	n=2	21%	32%	7%	5%	NA	NA
Sandy siltstone	Silt-sized grains of quartz and calcite. Mostly made of grains of calcite with minor to moderate quartz grains. Dominant cement is halite cement found in pores. Minor feldspar grains present.	Primary intergranular porosity is the dominant pore type but minor to moderate as a whole. Some secondary dissolution porosity is also present associated with carbonate grains.	Halite as pore-lining and pore-filling cement is the dominant cement in micro-facies. Additional cements include moderate carbonate cement and minor illite/ smectite cement in pores.	Grains: quartz, feldspar, calcite Cements: dolomite, calcite, illite/smectite, halite, pyrite Matrix: micrite	n=2	10%	35%	6%	39%	NA	NA

Table 1 | Sandstone to siltstone micro-facies. Micro-facies descriptions based on SEM and petrographic observations. Pore types and cements observed under SEM-EDS and petrography. Mineralogy percentages inferred from composite elemental data from SEM-EDS. Lab measured porosity and permeability by facies.

Micro-facies	Description	Pore types	Authigenic cements	Key components	Sample set	Mineralogy from EDS (%)				Lab Measured	
						Si	Ca	Al+K	Na+Cl	Porosity (%)	Permability (mD)
Il/S, dolomitic mudstone	Very fine-grained and clay matrix dominated with minor amounts of silt-sized grains of quartz and feldspars. Moderate amount of silt-sized dolomite present. Abundant horizontal delamination fracture and moderate vertical fractures. Fractures show minor to moderate cementation.	Dominant pore type is micro-porosity assoicated with authigenic cements in primary intergranular porosity. Additional pore type includes fracture porosity with minor to moderate authigenic cement fill.	Illite/smectite is the dominant cement in both the matrix and present as pore-lining to pore-filling cement. Secondary cements include haite and anhydrite as pore-filling cements and fracture fill cement.	Grains: dolomite, quartz Cements: illite/smectite, pyrite, halite Matrix: illite/smectite, micrite	n=4	28-43%	13-19%	>15%	<35%	17%	4.66 mD
Calcareous, silty mudstone	Very fine-grained calcite and quartz framework. Mostly calcite with quartz. Little to no feldspar present. Halite cement present in pores.	Abundant intergranular pores mostly clean of authigenic clays. Some intergranular pores doe have authigenic cements as pore-filling cements. Micro-porosity from authigenic clays is present. Moderate delaminated fractures present. Fracture porosity with variable authigenic cements present.	Minor to moderate illite/ smectie present in intergranular pores. Moderate amount of halite found in intergranular porosity and fracture porosity. Some dolomite cement.	Grains: calcite, dolomite, quartz Cements: illite/smectite, calcite, dolomite, pyrite Matrix: micrite	n=3	<45%	>30%	<15%	<35%	NA	NA
Calcareous, dolomitic mudstone	Very fine-grained calcite and quartz framework. Authigenic clays and dolomite cement present within pores. Little to no feldspar grains present. Halite cement present as pore-filling cement and fracture fill cement.	Minor to moderate primary intergranular porosity. Some secondary dissolution intragranular is present in carbonates. Moderate amount of fracture porosity with dissolution or vugs or pores.	Dolomite grains and cement present. Moderate amount of illite/smectite cement present in pores. Halite present as pore-filling and fracture filling cement.	Grains: calcite, dolomite Cements: calcite, dolomite, illite/smectite, pyrite Matrix: N/A	n=5	<45%	>30	<15%	<35%	3-8%	0.25-0.61 mD
Anhydritic-dolomudstone	Abundant dolomite and calcite present. Minor to moderate authigenic clays. Halite and anhydrite present as pore-filling cement and fracture filling cement.	Dominant primary intergranular porosity. Fracture porosity is present. Micro-porosity present when authigenic clays are present.	Dolomite grains and cement present. Moderate anhydrite and halite present as pore-filling cement and fracture-filling authigenic cement. Minor amount of illite/ smectite cement present in pores.	Grains: calcite, dolomite Cements: anhydrite, halite, calcite, dolomite, illite/smectite, pyrite Matrix: N/A	n=1	<45%	>30	<15%	<35%	3.50%	NA
Fossiliferous dolomudstone	Coarse skeletal bivalves present. Abundant calcite, dolomite, and halite. Very minor silica grains. Moderate to minor porosity, highly cemented.	Dominant primary intergranular porosity. Little to no micro-porosity due to lack of authigenic clays. Fracture porosity present but highly cemented.	Abundant halite cement as pore-filing and fracture-filling cement. Secondary calictie and dolomite cement. Little to no illite/smectite.	Grains: calcite, dolomite Cements: halite, calcite, dolomite, illite/smectite, pyrite Matrix: micrite	n=1	6%	33%	5%	30%	NA	NA

Table 2 | Mudstone and evaporitic micro-facies. Micro-facies descriptions based on SEM and petrographic observations. Pore types and cements observed under SEM-EDS and petrography. Mineralogy percentages inferred from composite elemental data from SEM-EDS. Lab measured porosity and permeability by facies.

Micro-facies	Description	Pore types	Authigenic cements	Key components	Sample set	Mineralogy from EDS (%)				Lab Measured	
						Si	Ca	Al+K	Na+Cl	Porosity (%)	Permability (mD)
Coarse crystalline halite	Abundant anhydrite and halite cement. Very minor fine to very fine quartz grains.	Mostly primary intergranular porosity.	Abundant anhydrite and halite cement. Little to no authigenic illite/smectite cement.	Grains: quartz, calcite, dolomite Cements: halite, calcite, dolomite, illite/smectite, pyrite Matrix: N/A	n=1	2%	21%	3%	42%	NA	NA
Nodular/ chicken wire anhydrite	Abundant anhydrite in forms of nodular morphs variable in size. Precipitated anhydrite in micritic matrix with organic matter present. Anhydrite also forms in silty mudstone matrix.	Mostly primary intergranular porosity.	Abundant anhdrite cement. Illite/smectite domains and cement.	Grains: quartz, calcite, dolomite Cements: anhdrite, calcite, dolomite, illite/ smectite, pyrite Matrix: illite/smectite, micrite	n=4	N/A	N/A	N/A	N/A	N/A	N/A
Laminated anhydrite	Abundant anhdrite in form of laminated or imbricated morphs. Precipitated laminated anhydrite present with micritc matrix.	Mostly primary intergranular porosity.	Abundant anhydrite cement with minor illite/smectite domains.	Grains: quartz, calcite, dolomite Cements: anhdrite, calcite, dolomite, illite/ smectite, pyrite Matrix: illite/smectite, micrite	n=2	N/A	N/A	N/A	N/A	N/A	N/A

Table 2 | Continued.

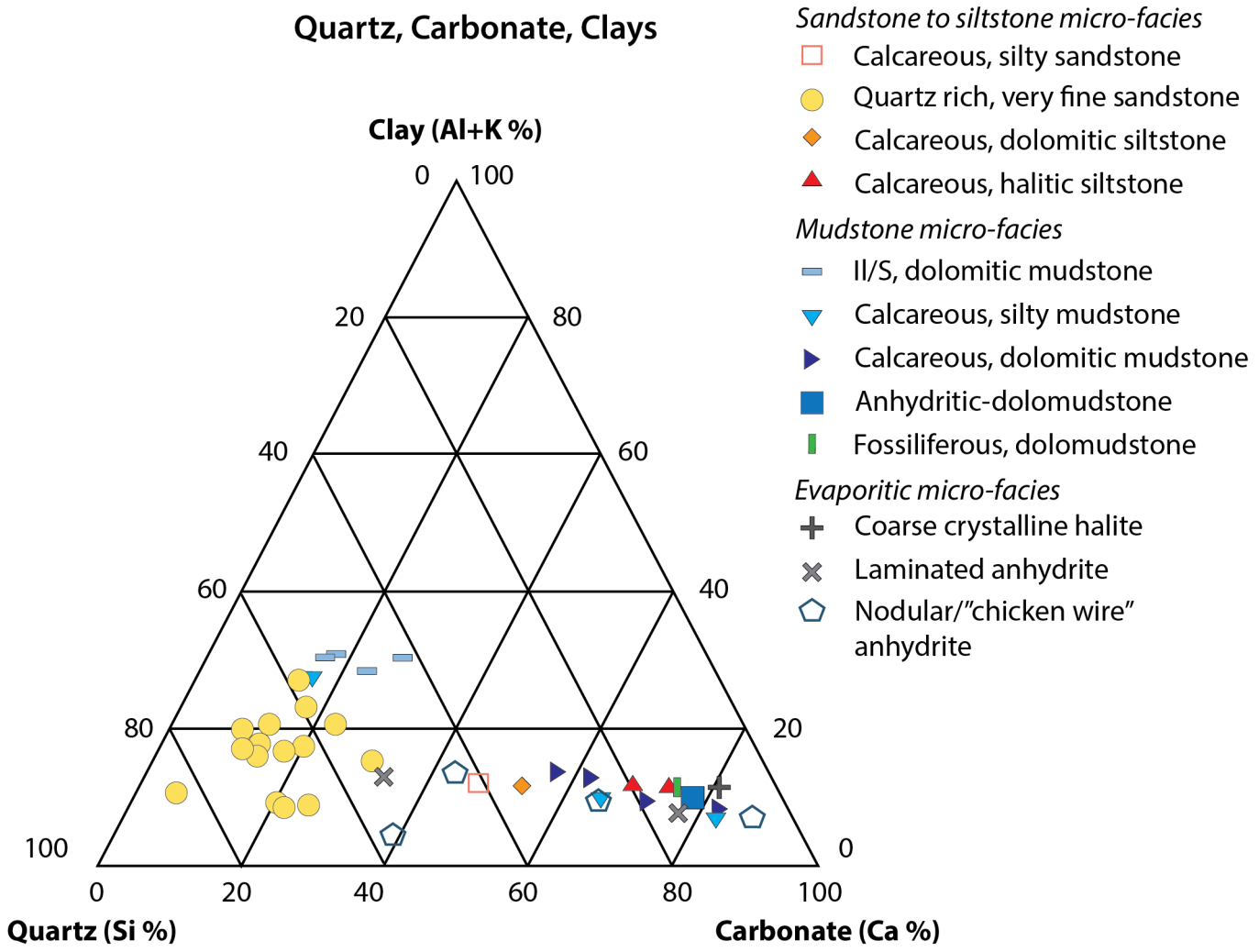

Figure 4 | Ternary diagram showing the ten identified micro-facies in this study. Ternary diagram based on quartz, carbonate, and clay percentages from composite elemental EDS maps. Quartz interpreted from silicon percent. Carbonate interpreted from calcium percent. Clay interpreted from aluminum and potassium percent.

with the micro-facies ordered accordingly from coarsest to finest grained: calcareous, silty sandstone; quartz-rich, very fine sandstone; calcareous, dolomitic siltstone; and calcareous, halitic siltstone (Figure 5A, D, G, J).

Quartz-rich, very fine sandstone micro-facies show the highest percent of illite/smectite of all the micro-facies (Table 1). Illite/smectite domains and cement are the dominant matrix with quartz grains being the dominant component in very fine sandstone micro-facies (Figure 5A–F). Illite/smectite clay domains form from a relatively continuous matrix surrounded by detrital grains (Yau et al., 1987). Calcite and dolomite are the dominant grains and cement with silt-sized quartz grains in calcareous, dolomitic siltstone micro-facies (Figure 5G–I). Primary intergranular porosity dominated by silt-size and clay domains and cement with secondary dissolution porosity is the dominant pore type in calcareous, silty sandstone, and in very fine sandstone micro-facies (Figure 6). Pore types in calcareous, sandy siltstone, quartz-rich, very fine sandstone, and calcareous, dolomitic siltstone micro-facies commonly have pore-filled to pore-lined clay cement due to the breakdown of siliciclastic grains resulting in precipitation of authigenic clay cement (Figures 5C, F, I and 6). Calcite and halite are the dominant grain and cement in calcareous, halitic siltstone micro-facies (Figure 5K, L). Pore types in calcareous, halitic siltstone micro-facies are generally low in authigenic clay cement and most pores appear to be secondary dissolution pores in dissolved carbonate grains (Figure 5L).

4.1.2. Mudstone micro-facies

Five identified mudstone micro-facies are characterized by fine-grained carbonate grains and illite/smectite clay matrix and cement. The mudstone micro-facies include (i) illite/smectite, dolomitic mudstone (n=4); (ii) calcareous, silty mudstone (n=3); (iii) calcareous, dolomitic mudstone (n=5); (iv) anhydritic-dolomudstone (n=1); and (v) fossiliferous dolomudstone (n=1) (Table 2) (Figures 7A–L and 8A–C). Evaporitic components (see evaporitic micro-facies section) can be found in mudstone micro-facies and vice versa. All mudstone micro-facies show less than 45% silicon in EDS maps (Table 2). Illite/smectite, dolomitic mudstone is the only mudstone micro-facies with over 35% illite/smectite (Table 2) (Figure 7A–C). Primary intergranular porosity is the dominant pore type in dolomitic mudstone micro-facies (Figure 9A–D). Pores

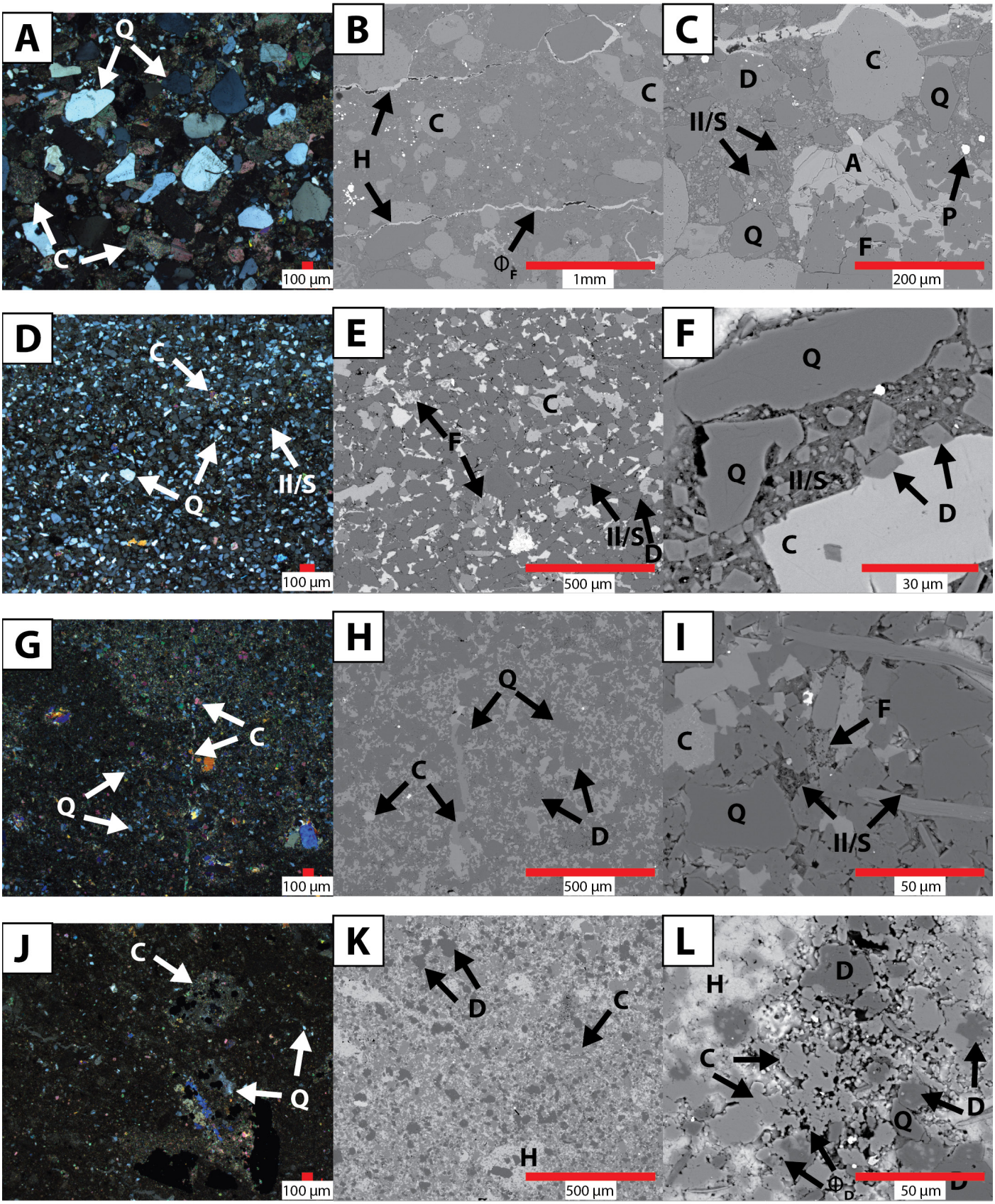

Figure 5 | Petrographic and SEM analyses of sandstone to siltstone micro-facies. (A–C) Calcareous, silty sandstone; 2,951 m (9,682.2′). (D–F) Quartz-rich, very fine sandstone micro-facies; 2,989 m (9,706.9′). (G–I) Calcareous, dolomitic siltstone micro-facies; 2,947 m (9,669.7′). (J–L) Calcareous, halitic siltstone micro-facies; 2,968 m (9,736.8′). (Q) Quartz, (C) Calcite, (D) Dolomite, (F) Feldspar, (Il/S) Illite/smectite, (H) Halite, (P) Pyrite, and (A) Anhydrite.

are either pore-lined to pore-filled by clay or authigenic cements. Additional pore types in mudstone micro-facies include micropores (<62.5 µm) between clay domains and cements and organic matter nanopores (<1 µm) in mudstone micro-facies (Figure 9C, D) (Loucks et al., 2012).

The other four mudstone micro-facies show less than 15% illite/smectite (Table 2).

Calcareous, silty mudstone (n=3) and calcareous, dolomitic mudstone (n=5) micro-facies are very similar in

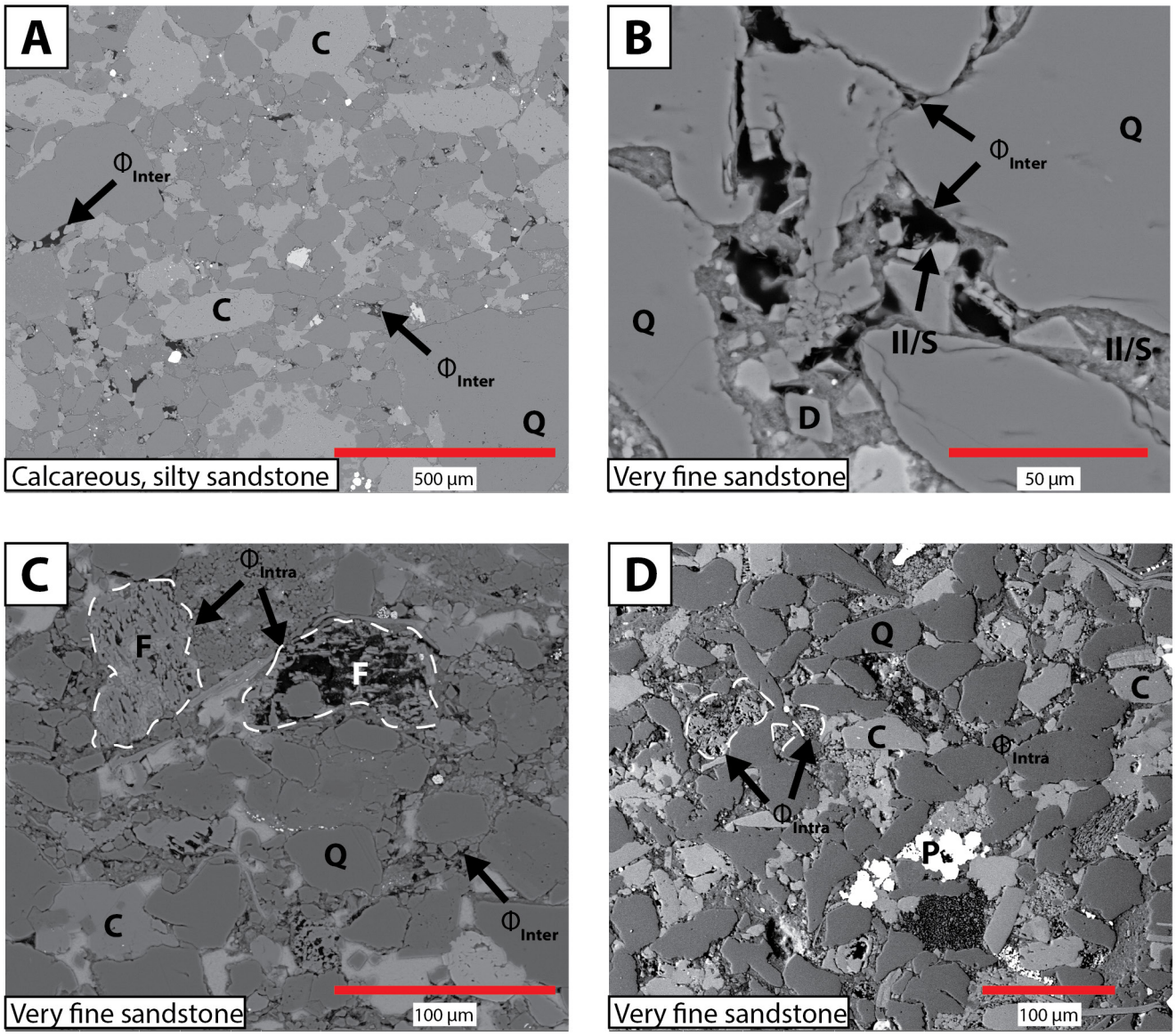

Figure 6 | Dominant pore types in sandstone to siltstone micro-facies from backscatter SEM micrographs. (A) Calcareous, silty sandstone characterized by intergranular porosity. (B) Quartz-rich, very fine sandstone characterized by intergranular porosity with illite/smectite clay domains, cement, and dolomite. (C) Quartz-rich, very fine sandstone showing intragranular dissolution pores in feldspars with primary intergranular porosity. (D) Quartz-rich, very fine sandstone showing intragranular dissolution pores in feldspars. (Q) Quartz, (C) Calcite, (D) Dolomite, (F) Feldspar, (Il/S) Illite/smectite, (P) Pyrite, (Φ_{inter}) intergranular porosity, and (Φ_{intra}) intragranular porosity.

quartz, carbonate, and clay content (Table 2). Dolomitic mudstone micro-facies commonly have a low abundance of illite/smectite cement due to the lack of siliciclastics (i.e., feldspar or quartz) (Figure 7C, F, I, L). Anhydritic-dolomudstone micro-facies is similar to other dolomitic mudstone micro-facies but anhydrite is generally present as nodules or cements (Figure 7J). Anhydritic-dolomudstone (n=1) micro-facies primary intergranular porosity with varying degrees of pore-lined to pore-filled cementation (Figure 7K, L). Fossiliferous dolomudstone (n=1) micro-facies has calcite present as skeletal bioclast fossils, grains, and cement (Figure 9A–C). Primary intergranular porosity generally lacks clay cement due to dominant carbonate composition and siliciclastic input.

4.1.3. Evaporitic micro-facies

The evaporitic micro-facies are characterized by halite and anhydrite and include (i) coarse, crystalline halite (n=1); (ii) laminated anhydrite (n=2); and (iii) nodular anhydrite (n=4) (Table 2) (Figure 9).

Coarse crystalline halite micro-facies is predominately composed of precipitated crystalline halite (42%) (Table 2; Figure 8D, F). Coarse crystalline halite micro-facies also include anhydrite and minor amounts of quartz and dolomite grains (Figure 8E, F). Pore types generally include intercrystalline porosity (Figure 8E, F).

Nodular anhydrite (also known as "chicken wire" anhydrite) and laminated anhydrite micro-facies are observed as varying anhydrite morphologies surrounded by silty and dolomitic matrix (Figure 9G–L). Grains can be both siliciclastic and carbonate grains as anhydrite is observed in both very fine-grained sandstone, siltstone, and dolomitic mudstone micro-facies. Anhydrite precipitated as a displacive cement, interpreted as in-situ within the sediment and surrounded by clay and carbonate matrix.

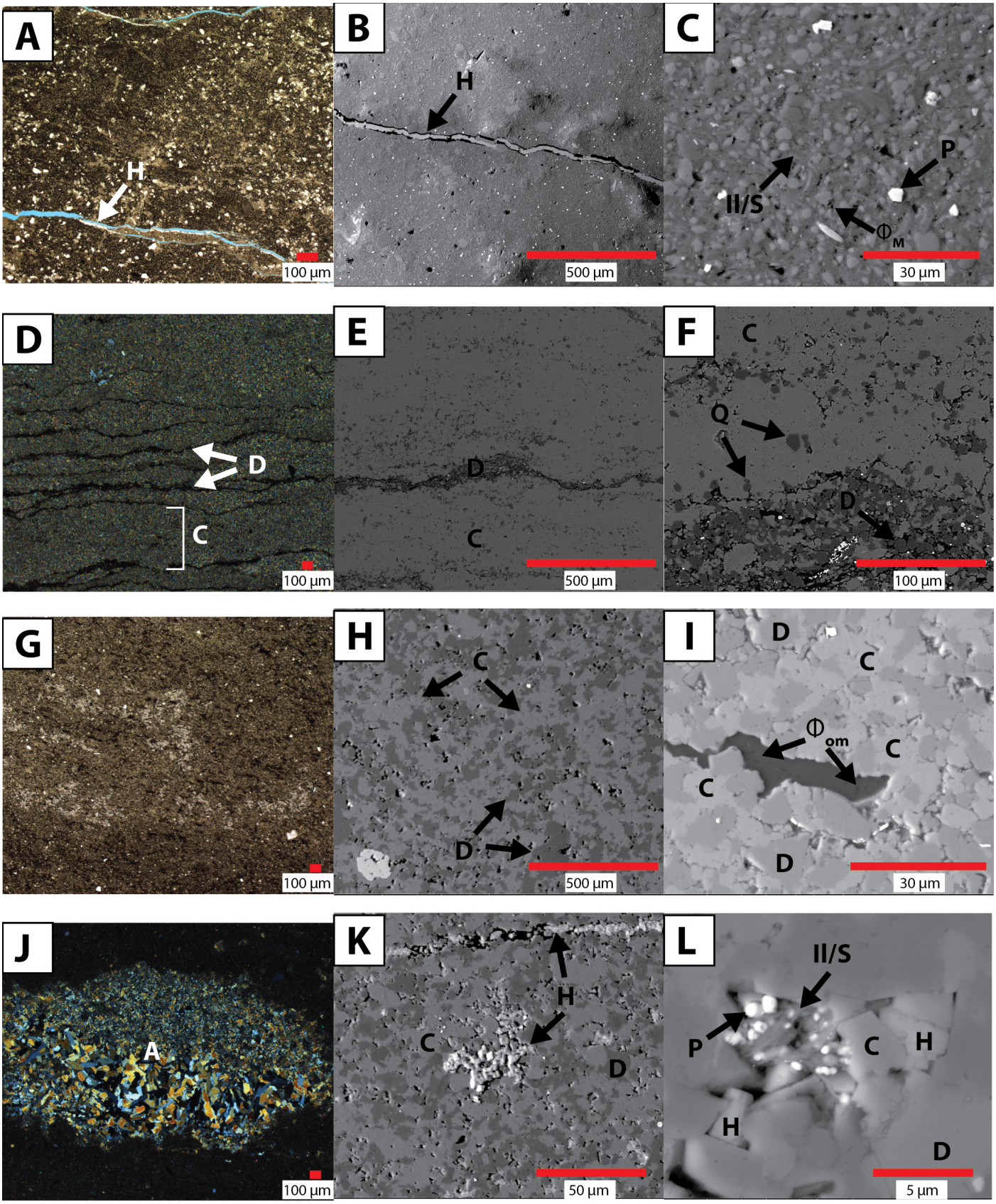

Figure 7 | Petrographic and SEM images of mudstone micro-facies. (A–C) Illite/smectite, dolomitic mudstone micro-facies; 9,686 m (9,685.9′). (D–F) Calcareous, silty mudstone micro-facies; 2,941 m (9,648.7′). (G–I) Calcareous, dolomitic mudstone micro-facies; 2,944 m (sample #9658.1). (J–L) Anhydritic-dolomudstone micro-facies; 2,940 m (sample #9644.1). (Q) Quartz, (C) Calcite, (D) Dolomite, (F) Feldspar, (II/S) Illite/smectite, (H) Halite, (P) Pyrite, (A) Anhydrite, and (Φ_{om}) Organic-matter pores.

The sulfur percent associated with anhydrite is commonly over 20% in evaporitic micro-facies. Depending on the degree of magnification of a sample, anhydrite can represent between 30 to over 90% of a petrographic image. Laminated anhydrite micro-facies show abundant precipitated anhydrite with laminated and imbricated morphologies typically in a silty-dolomitic matrix (Figure 9J–L).

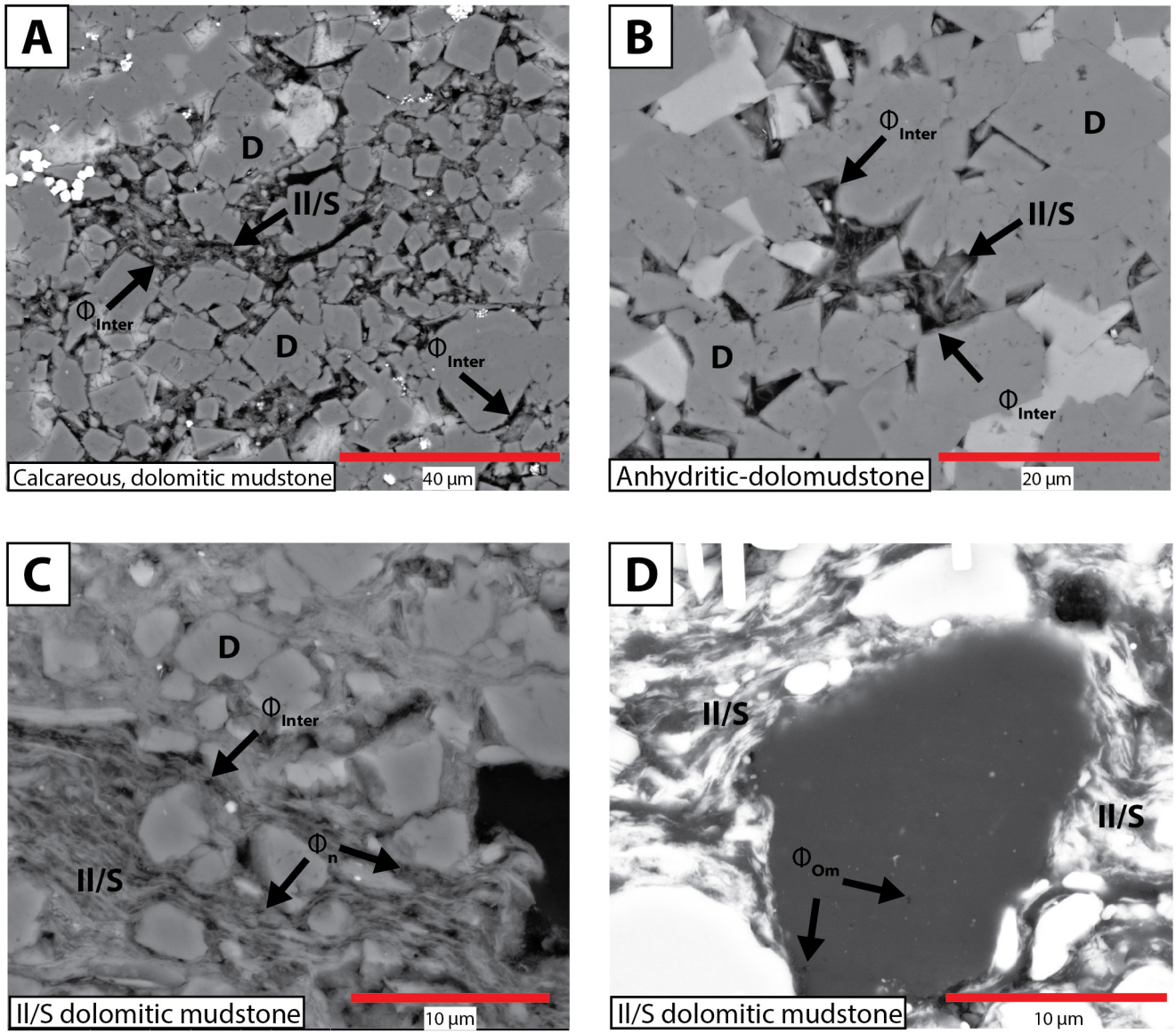

Figure 8 | Dominant pore types in mudstone micro-facies from backscatter SEM micrographs. (A) Calcareous, dolomitic mudstone characterized by intergranular porosity. (B) Anhydritic-dolomudstone characterized by intergranular porosity with illite/smectite clay domains, cement, and dolomite. (C) Illite/smectite dolomitic mudstone characterized by intergranular and nanopores in illite/smectite domains. (D) Illite/smectite dolomitic mudstone characterized by nanopores in illite/smectite domains and nanopores in organic matter. (Q) Quartz, (C) Calcite, (D) Dolomite, (F) Feldspar, (Il/S) Illite/smectite, (Φ_{inter}) intergranular porosity, (Φ_{n}) nanopores and (Φ_{om}) organic matter nanopores.

4.2. Porosity/permeability trends and interpretation by micro-facies

4.2.1. Micro-facies porosity/permeability trends

Porosity and permeability measurements (n=62) from conventional core analysis were available for the core interval. Porosity and permeability measurements were integrated with identified micro-facies and lithofacies core descriptions to evaluate porosity and permeability trends (Figure 10). Some samples were reported as "partially fractured" (n = 34) given the Cane Creek Shale's state of stress anisotropy likely induced during coring (McCormack et al., 2023). Fractured samples were omitted from the analysis (Figure 10B). Intact samples capture the range of permeability in the dataset with variable porosity over ~11% in partially fractured samples, likely not representative of the Cane Creek Shale (Figure 10B), although Grove et al. (1993) reported permeabilities from 39 to 400 md for the Cane Creek Shale, in range of samples from this study.

Quartz-rich, very fine sandstone micro-facies consistently show ideal moderate to high porosity and moderate to high permeability values (Figure 10B). Porosity values range from ~2 to 11%. Permeability in quartz-rich, very fine sandstone micro-facies ranges from ~0.003 to ~30 mD (Figure 10B). Permeability values in the quartz-rich, very fine sandstone micro-facies are generally some of the highly measured data. Dominant pore types in the quartz-rich, very fine sandstone micro-facies are primary intergranular porosity with pore-lined to pore-filled clay cements, and some secondary grain dissolution intragranular porosity (Figure 5E, F). The primary intergranular porosity, with variable degrees of clay domains and cements, contributes to hindering the quartz-rich, very fine sandstone microfacies' porosity and permeability.

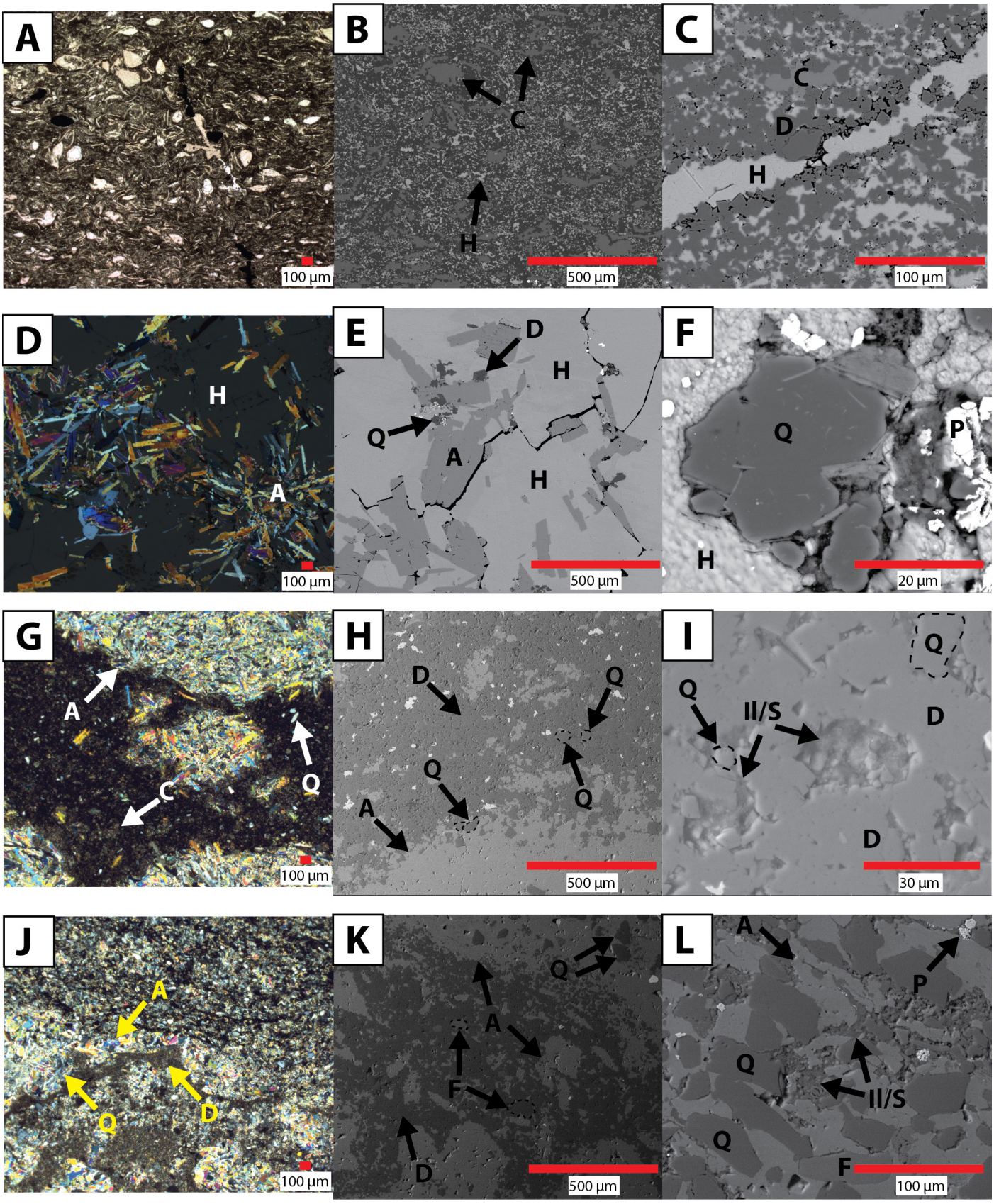

Figure 9 | Petrographic and SEM micro-facies. (A–C) Fossiliferous dolomitic mudstone micro-facies; 2,968 m (9,736.1'). (D–F) Coarse crystalline micro-facies; 2,966 m (9,729.8'). (G–I) Nodular/ "chicken wire" anhydrite micro-facies; 2,942 m (9,653.35'). H. Nodular anhydrite; 2,957 m (9,700.75'). (I–J) Laminated anhydrite micro-facies; 2,943 m (9,655.6'). (Q) Quartz, (C) Calcite, (D) Dolomite, (F) Feldspar, (Il/S) Illite/smectite, (H) Halite, (A) Anhydrite, and (P) Pyrite.

Siltstone micro-facies such as calcareous, dolomitic siltstone and calcareous, halitic siltstone commonly exhibit primary intergranular porosity with pore-lined to pore-filled cement and secondary dissolution intragranular porosity in feldspar and carbonate grains (Figure 5I, L). Siltstone secondary dissolution intragranular porosity is associated with the abundance of feldspars and carbonates with varying degrees of dissolution. Intergranular porosity is commonly found with pore-filling or pore-lining clays (Figure 5I). Permeability in siltstone micro-facies is

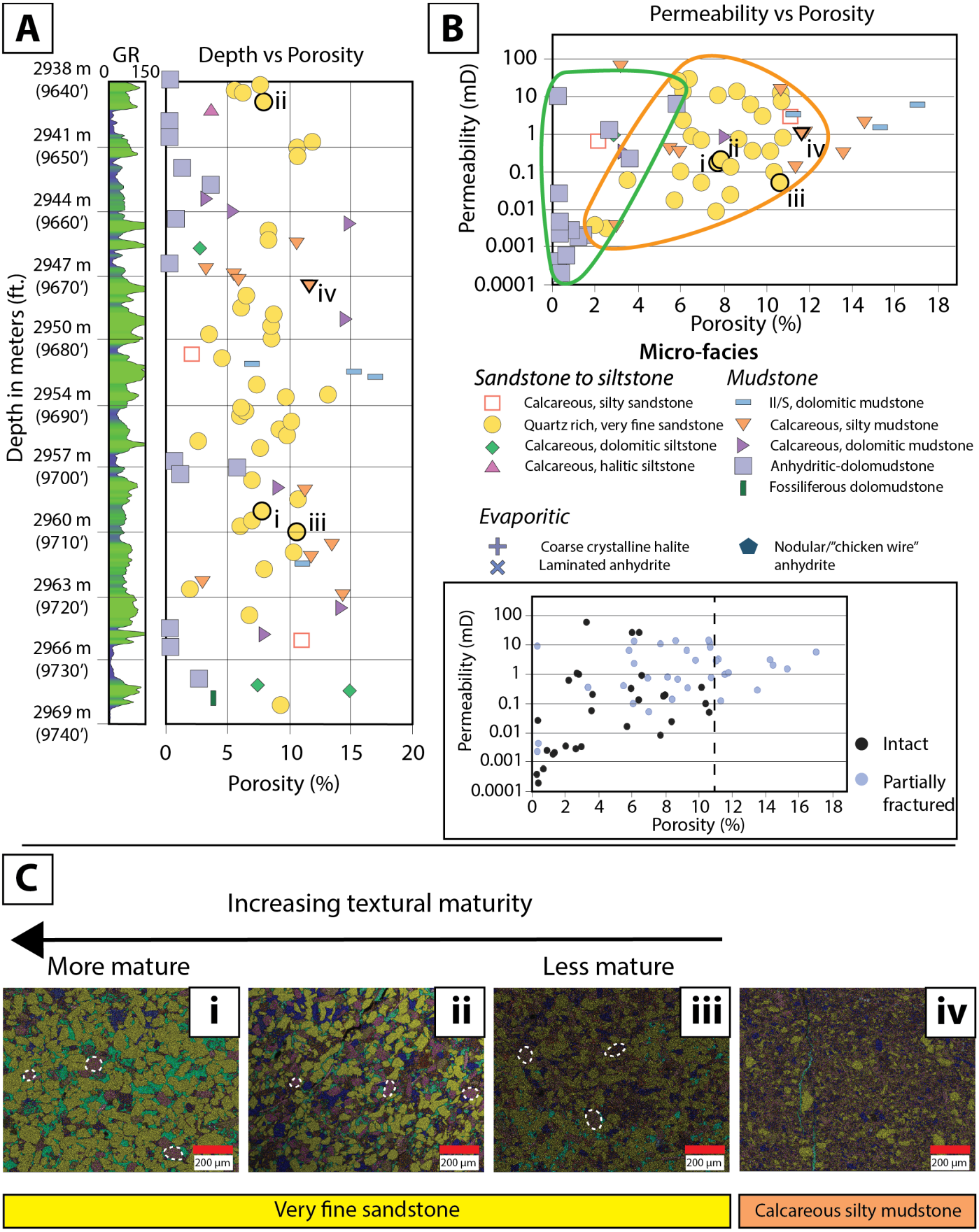

Figure 10 | Porosity and permeability trends with micro-facies from SEM. (A) Depth versus Porosity chart with gamma-ray (GR) log. (B) Permeability versus Porosity chart. Subset image. Intact and partially fractured core plugs reported for porosity and permeability. Dashed line showing 11 % porosity. (C) SEM with EDS samples showing increasing textural maturity in quartz-rich, very fine sandstone micro-facies (i, ii, and iii) with calcareous silty mudstone for comparison (iv). Feldspars are outlined in i, ii, and iii.

reduced by illite/smectite cement within available pore space.

Dolomitic mudstone micro-facies consistently show low porosity and permeability values with representative porosity being <2% and permeability being <0.01 mD and

some anomalously high values (Figure 10B). Dolomitic mudstone including anhydritic-dolomudstone and calcareous, dolomitic siltstone, micro-facies show low porosity values between <1 to ~6%. Permeability for dolomitic mudstone micro-facies in general have permeabilities an order of magnitude lower than sandstone micro-facies (Figure 10B). Dolomitic mudstone micro-facies have low to moderate values (~0.0002 to ~10 mD) with <0.01 mD characteristic of this microfacies (Figure 10B).

The dominant pore type in the dolomitic mudstone micro-facies is primary intergranular porosity with varying degrees of micro-porosity associated with pore-filling and pore-lining clay micro-porosity. Anhydritic-dolomudstone varies from other dolomitic mudstone micro-facies in that a greater abundance of anhydrite is present as nodules or pore-filling cement (Figure 7J). The dominant pore type in anhydritic-dolomudstone is primary intergranular porosity. Illite/smectite, dolomitic mudstone micro-facies show some of the highest porosity values (>15%) (Figure 10A). Similarly, the illite/smectite, dolomitic mudstone sample shows the highest permeability value of the dataset (4.66 mD) (Figure 10B). The dominant pore type in the illite/smectite, dolomitic mudstone micro-facies is halite-cemented fracture porosity (Figure 7A, B). Additional pore types, likely representative of in-situ matrix porosity and permeability, include primary intergranular porosity and moderate micro-porosity associated with pore-lined to pore-filled clays (Figure 9A, B).

4.2.2. Micro-facies interpretations

The ~10% range variability in porosity in quartz-rich, very fine sandstone micro-facies is generally controlled by the mineralogical maturity. Mineralogical maturity here refers to the abundance of quartz to feldspars where a higher maturity indicates a more quartz-rich sample (Folk, 1954). The lack of feldspars and clay cements allows for the precipitation of alternative cements like halite cement. Such cements can occlude intergranular porosity thus reducing permeability by minimizing effective porosity (Figure 10C). Low porosity and permeability can also be affected by the compaction of grains reducing the interconnected pore network. Samples abundant in feldspars and clay cements are considered less mineralogically mature and typically exhibit higher porosity values (Figure 10A, B, C). Higher porosity is characterized by a stable siliciclastic grain sorting with intergranular porosity and enhanced intragranular porosity in clay domains. (Figure 10C).

The low porosity and permeability in dolomitic mudstone micro-facies are likely controlled by moderate to well-sorted carbonate grains. The abundance of carbonate and well-sorting in calcareous, dolomitic-mudstone preserves a porosity network but lacks good interconnectivity. The abundance of interlocking, crystalline calcite and dolomite and lack of feldspars and siltstones, minimizes nucleation and solutes necessary for authigenic cement growth, reducing permeability in siltstone micro-facies (i.e., hinders the development of pore filling illite/smectite). Hence, the lack of authigenic clays is correlated to the lack of available feldspars and silica in these mudstone facies. Feldspar and quartz abundance in the micro-facies leads to the precipitation of illite/smectite authigenic clays through silica and aluminum mobility (Taylor & Macquaker, 2014). Minor authigenic clay solutes can be supplied by highly reactive clay detritus from adjacent mudstone micro-facies. Additional pore types include micro-porosity associated with pore-filling and pore-lining authigenic cements (i.e., anhydrite, halite, and illite/smectite). The high degree of cements in available pore space greatly reduces porosity values.

The high porosity and permeability values of illite/smectite, dolomitic mudstone micro-facies are likely a result of delamination fractures associated with sample damage during preparation (and/or drilling) (Figures 7A, B and 10A, B). Induced fracture porosity primarily controls measured permeability in illite/smectite, dolomitic mudstone micro-facies. Fractures in illite/smectite, dolomitic mudstone micro-facies commonly show halite cementation, so these fractures may exist in the subsurface. Sample damage and delamination make it difficult or impossible to discern the original fracture porosity (Figure 10B).

4.3. Paragenetic sequence

A paragenetic sequence for the Cane Creek Shale of the Paradox Formation was developed for the northern portion of the Paradox Basin, southeastern Utah. The paragenetic sequence was developed by describing detrital and authigenic relationships observed from petrography and SEM with EDS composite elemental maps. Observed cross-cutting relationships between detrital and authigenic mineral cementation provide a relative timing of diagenetic events described as Early (eogenetic), Middle (mesogenetic), and Late (telogenetic) stages for the Cane Creek Shale (Figure 11). Eogenetic refers to the time of pre-burial post deposition, mesogenetic refers to the time of deeper burial, and telogenetic refers to the late stage (Choquette & Pray, 1970).

4.3.1. Early stage (Eogenetic)

The Early, eogenetic stage coincides with physical changes including compaction and grain rotation, and a series of geochemical authigenic cementation events including calcite, dolomite, illite-smectite clays, and quartz overgrowths. Evidence for grain compaction is most apparent in the sandstone to siltstone micro-facies and varies in the degree of compaction features from grain contacts, sutures, and grain fractures (Figure 12A, B). Physical processes associated with compaction include grain rearrangement by frictional slip and rotation, grain crushing and fracturing, ductile grain deformation, and physical-chemical processes such as pressure dissolution at grain contacts (Karner et al., 2005; Milliken & Olson, 2017). While there is evidence for moderate compaction in

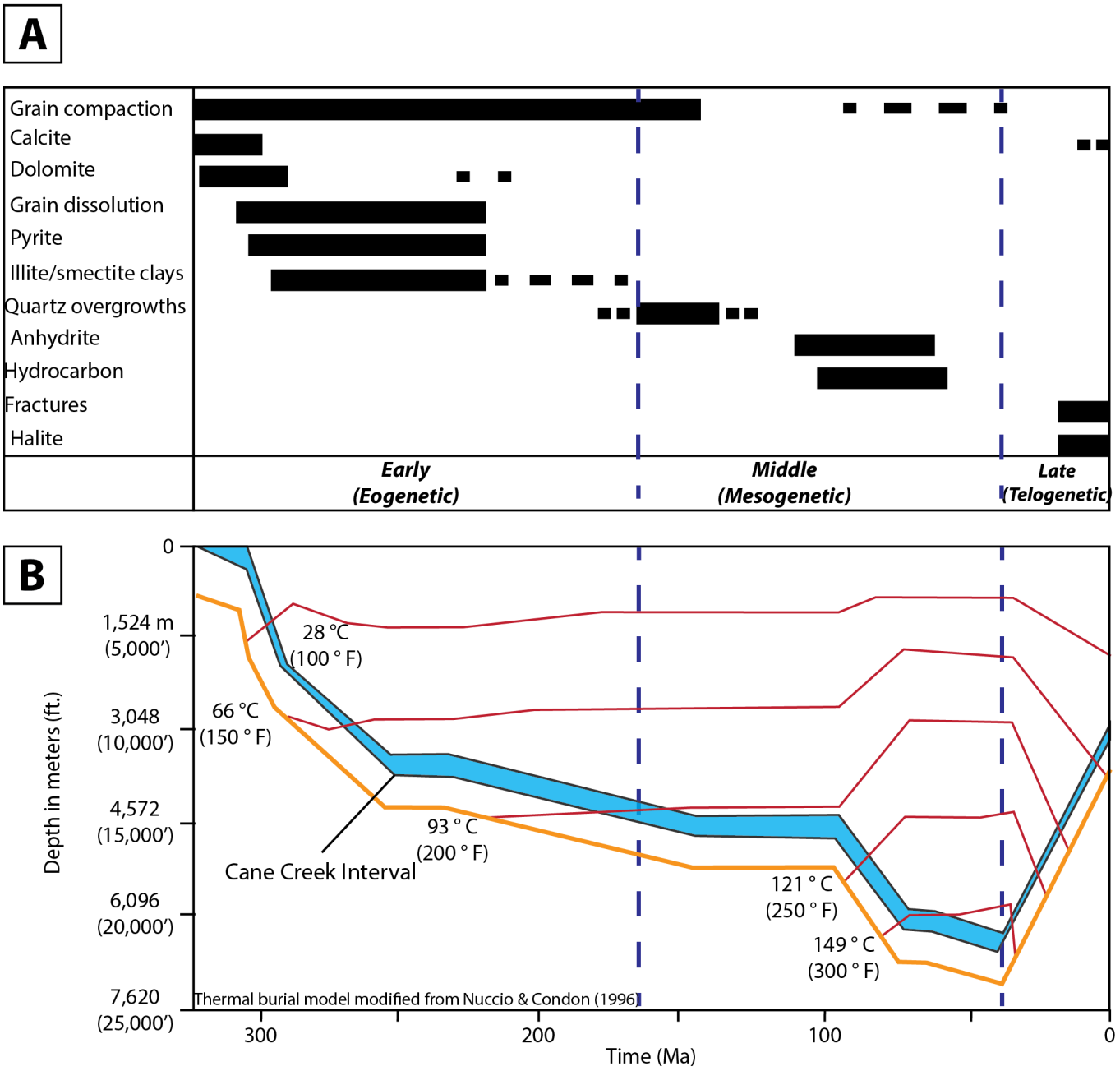

Figure 11 | (A) Paragenetic Sequence based on petrography and SEM of the Cane Creek Shale. See text for early, middle, and late-stage diagenetic event definitions. (B) Thermal burial and hydrocarbon generation model modified from Nuccio & Condon (1996). See Nuccio & Condon (1996) for thermal burial model inputs.

the Cane Creek interval, evidence for extreme compaction is lacking. Extreme chemical compaction features such as styolitic grain textures are not observed. The moderate compaction is likely due to gradual burial during the Early stage.

The paragenetic sequence during the Early stage is characterized by the precipitation of several authigenic minerals, suggesting early syn-depositional origin, and grain dissolution (Figure 11A). The first of these authigenic cements are associated with early depositional and diagenetic dolomite and calcite crystallization (Figure 12C, D). The majority of the dolomite in the Cane Creek Shale is precipitated fine-grained euhedral crystals varying in size from ~2-20 μm. The dolomite has a planar to non-planar texture (Figure 12C, D) and is found as displacive cement within illite/smectite, suggesting early-stage penecontemporaneous precipitation during fine-grained deposition (Figure 12E). Diagenetic euhedral dolomite crystals are observed predating later-stage cements such as halite and illite/smectite (Figure 12A, D). Additional early cements such as pyrite, although minor in abundance, is observed as clustered and individual framboids (Figure 13C–F). Pyrite clusters can also be found along with illite/smectite cements indicating precipitation following early deposition.

Fine-crystalline dolomite in illite/smectite domains likely resulted from sulfate reduction and methanogenesis in the pore waters and deposited mud sediments (Curtis & Coleman, 1986; Taylor & Macquaker, 2014). The precursor of carbonate here defines the fine-crystalline dolomitic grain sizes found in the Cane Creek Shale (Haeri-Ardakani et al., 2013) (Figure 12E, F). Micro-facies rich in carbonate

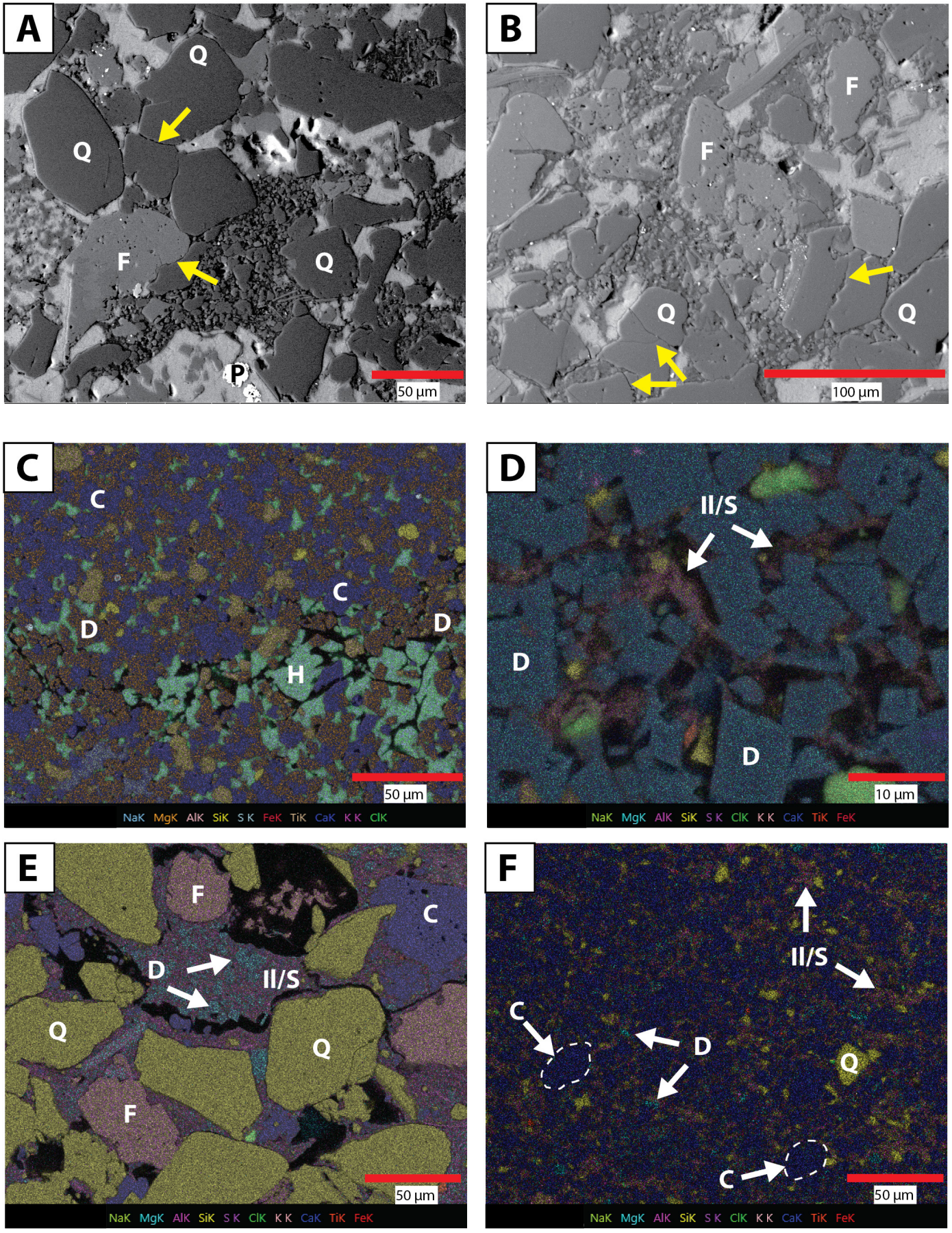

Figure 12 | SEM petrographs with composite elemental EDS maps. (A) Quartz-rich, very fine sandstone micro-facies showing evidence for feldspar dissolution developing micro-pores. Compaction features shown as grain contacts and suturing (yellow arrows); 2,939 m (9,642.9'). (B) Quartz-rich, very fine sandstone micro-facies showing feldspar dissolution micro-pores and evidence for compaction as grain fractures (yellow arrows); 2,939 m (9,642.9'). (C, D) Calcareous, halitic siltstone and calcareous, dolomitic siltstone micro-facies showing carbonate and dolomite grains. Note minor authigenic clays in pore network; 2,940 m and 2,947 m (9,644.1' and 9,669.7'). (E) Quartz-rich, very fine sandstone with early dolomite cement precipitating in illite/smectite domains; 2,960 m (9,711.9'). (F) Illite/smectite micro-facies with illite/smectite domains and dolomite and clay cements; 2,952 m (9,683.85'). (Q) Quartz, (C) Calcite, (D) Dolomite, (F) Feldspar, (Il/S) Illite/smectite, (H) Halite, and (P) Pyrite.

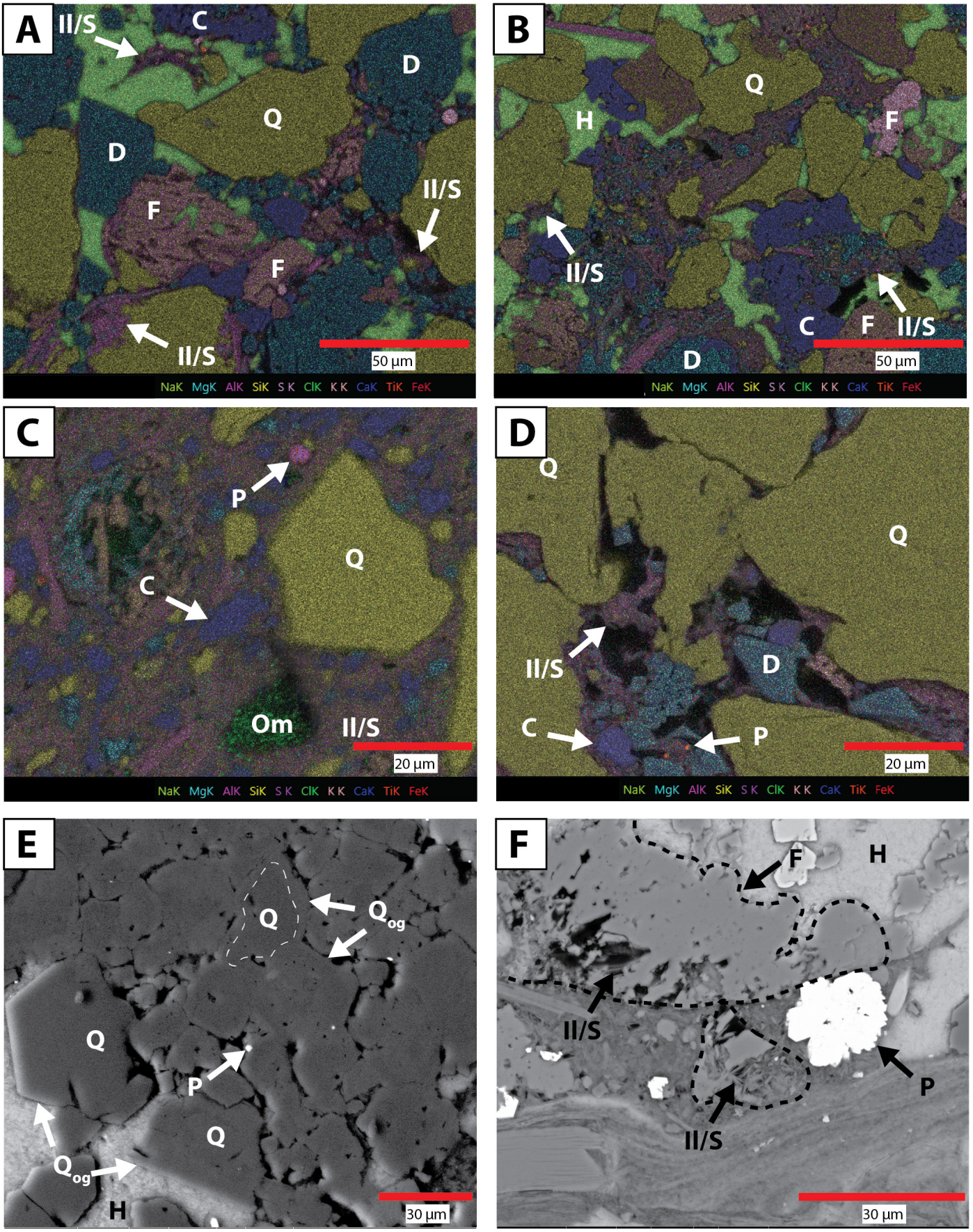

Figure 13 | SEM petrographs with composite elemental EDS maps. (A, B) Quartz-rich, very fine sandstone micro-facies showing feldspar dissolution porosity and abundant authigenic clay cement; 2,939 m and 2,939 m (9,642.2′ and 9,643.5′). (C, D) Quartz-rich, very fine sandstone micro-facies showing minor authigenic pyrite with illite/smectite cements; 2,953 m and 2,960 m (9,689′ and 9,710.4′). (E) Quartz-rich, very fine sandstone micro-facies showing earlier quartz grains with later planar quartz overgrowths. Note lack of feldspars and authigenic clay cements; 2, 939 m (9,642.9′). (F) Quartz-rich, very fine sandstone micro-facies with abundant clay cement, dissolved feldspar grain, and minor quartz overgrowths 2,954 m (9,692.7′). (Q) Quartz, (Qog) Quartz overgrowth, (C) Calcite, (D) Dolomite, (F) Feldspar, (Il/S) Illite/smectite, (H) Halite, (P) Pyrite, and (Om) Organic matter.

material typically lack abundant authigenic clay cements due to the low abundance of siliciclastic grains (i.e., feldspar and quartz) (Figure 12C, D).

Illite/smectite is observed as clay domains and pore-filling authigenic cement. During the Early stage, the dissolution of feldspar in sandstone to siltstone micro-facies promoted illite/smectite clay precipitation as part of the early paragenetic sequence (Figures 12A, B, D and 13A, B). The breakdown and solid solution of feldspars and mica supplied available K and Al for illite/smectite transformation. Minor quartz overgrowths served as a sink for silica in the illite/smectite transformation (Figure 13C, D) (Awwiller, 1993; Huggett, 1996).

Pyrite cement precipitated in the early paragenetic sequence during the Early stage. Minor pyrite cement is likely the result of anaerobic oxidation in minimal oxygen-free conditions within pore waters in sediments (Raiswell, 1982). The anaerobic oxidation reactivity from organic matter within sediments or more specifically sulfate reduction led to pyritization in a reducing environment (Berner, 1970; Taylor & Macquaker, 2000; Macquaker et al., 2014; Fishman et al., 2015). Limited oxygen during reducing conditions allowed for microbial sulfate reduction further depleting oxygen (Fishman et al., 2015). Pyrite is commonly observed as displacive framboids in illite/smectite domains (Figure 13C, F). The morphology of framboids is controlled by the diagenetic occurrence of pyrite (Raiswell, 1982; Taylor & Macquaker, 2000). Pyrite precipitation likely consumed any reactive iron flux within the sediments, resulting in minor pyrite framboids (Figure 13C–F).

4.3.2. Middle stage (Mesogenetic)

A series of authigenic cementation events, mainly quartz overgrowths and authigenic anhydrite, characterize the Middle, mesogenetic stage of the paragenetic sequence. In the Middle stage, authigenic cements are generally less extensive than in the Early stage. Quartz cement, although present, is not a major constituent in the Cane Creek Shale (Figure 13E, F). The final authigenic cementation event in the middle stage is anhydrite cement precipitation following illite/smectite and quartz development. Anhydrite cement usually occurs as a later pore-filling cement (Figure 14A, B).

Though minor, the first Middle stage diagenetic event is the development and nucleation of quartz overgrowths. Quartz overgrowths are observed as predating later-stage authigenic cements such as illite/smectite and halite (Figure 13A, B, E). Quartz overgrowths or cementation is negligible or slow below 100 °C (212 °F) (Giles et al., 1992; Huggett, 1996). Quartz development likely did not initiate during the Early stage as burial temperatures were not elevated enough in the Paradox Basin to initiate quartz nucleation. Additionally, the high degree of illite/smectite authigenic cement in sandstone to siltstone micro-facies likely did not allow quartz to nucleate on surfaces, precluding the development of extensive quartz overgrowths (Figure 13, F). Milliken & Olson (2017) suggested some possible routes for silica digenetic precipitation that include pressure solution of detrital quartz, feldspar dissolution, illitization of smectite, biogenic opal, and volcanic glass. Given the geologic context, biogenic opal derived from radiolarians and volcanic glass was discarded. Minor quartz overgrowths postdate feldspar dissolution and illitization of smectite leading to silica solutes required for a minor amount of quartz cement. Some minor silica could also have been put into solution by minor pressure solution brought on by grain fracturing leading to hydrostatic levels of fluid pressures leading to a small amount of quartz cement (Makowitz et al., 2006).

Hydrocarbon generation was the latest event described in the paragenetic sequence in the Cane Creek Shale during the Middle stage. Organic matter identified from SEM shows evidence of kerogen cracking and organic matter porosity generation from hydrocarbon generation (Figure 14C, D). Organic matter fabric shows the generation of micropores, organic matter fracture porosity, and withdrawal pores between organic matter and matrix/grains (Figure 14C, D). Given the size of these micropores, liquid hydrocarbons may be stored yet pore connectivity is minimal. Larger interconnected, gas bubble pores, not observed here, may indicate more mature hydrocarbons such as natural gas (Milliken et al., 2013; Löhr et al., 2015).

4.3.3. Late stage (Telogenetic)

Only two major diagenetic events led by fracture initiation and halite and late calcite vein precipitation characterize the Late, telogenetic stage paragenetic sequence. Many of the Cane Creek Shale cross-cutting fractures are associated with some degree of halite-filled cementation. Halite cementation and calcite-filled veins are Late stage diagenetic events commonly associated with either fracture-fill or pore-filling cementation (Figure 14A, B, E, F). Calcite-filled veins are observed cross-cutting early dolomite followed by a later stage anhydrite pore-filling cementation and finally by halite cement (Figure 14B). Calcite-filled veins are relatively minor in abundance compared to halite-filled veins. Two types of fractures in the Cane Creek Shale include: 1) in-situ vertical to subvertical fractures, and 2) induced horizontal or delamination fractures, likely resulting from drilling and sample preparation (Figure 14E, F).

5. Discussion

5.1. Depositional factors on diagenesis

Detailed micro-facies characterization of the Cane Creek Shale interval highlights a coeval, carbonate, and siliciclastic, fine-grained depositional environment characterized by clastic and evaporitic cyclic deposition in a sabkha type environment (up to 80 cycles in the Hermosa Group)

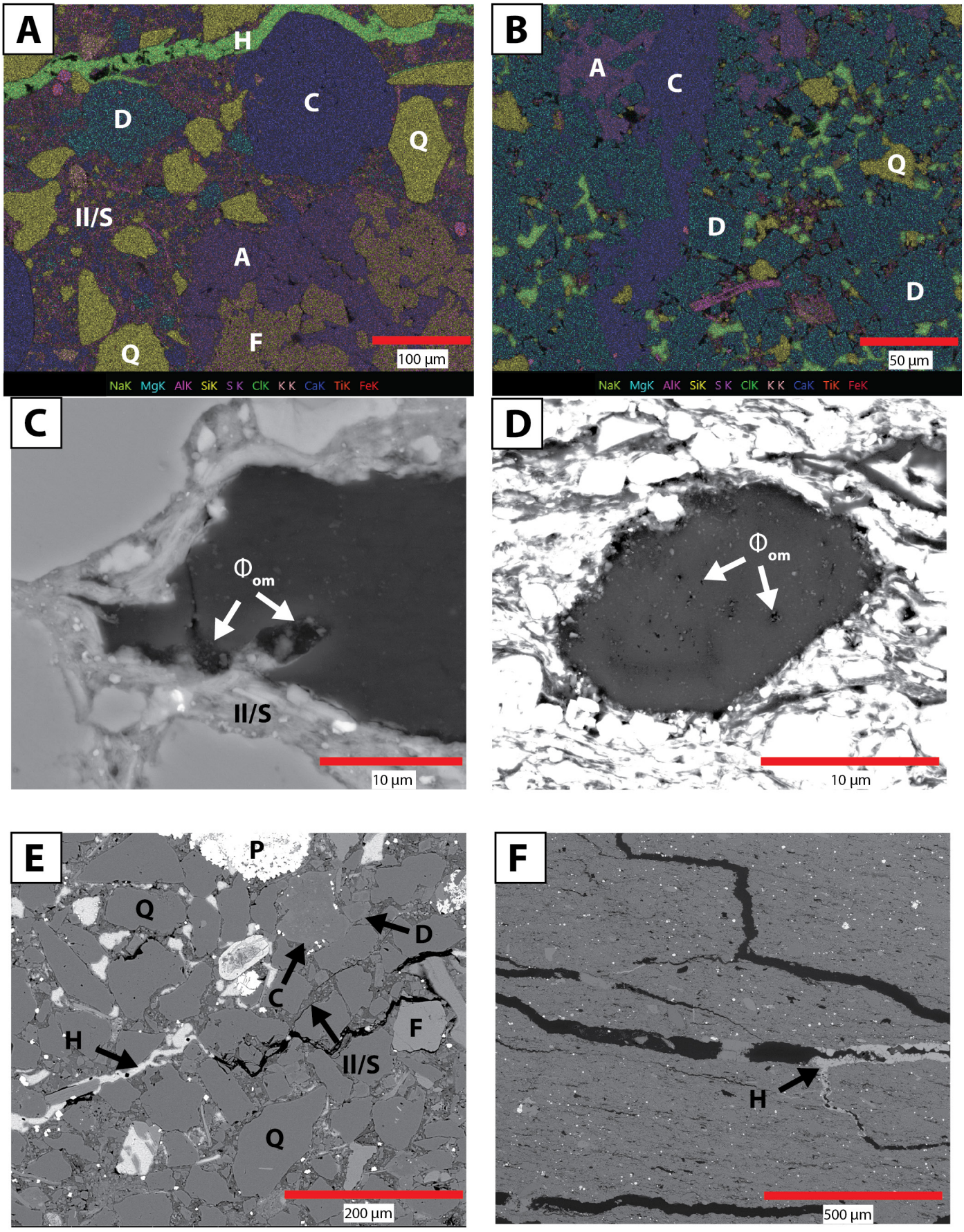

Figure 14 | SEM petrographs with composite elemental EDS maps. (A) Calcareous, silty sandstone micro-facies with abundant quartz, feldspar, and carbonate grains with pore-filling illite/smectite clay cement and anhydrite cement; 9,682.2 m (9,682.2′). (B) Calcareous, dolomitic siltstone micro-facies with pore-filling anhydrite and carbonate vein cements; 2,947 m (9,669.7′). (C, D) Organic matter in quartz-rich, very fine sandstone and illite/smectite dolomitic mudstone micro-facies. Note organic matter porosity and cracking in both SEM micrographs; 2,948 m and 2,950 m (9,672.2′ and 9,677.2′). (E) Quartz-rich, very fine sandstone micro-facies with partially filled halite-cemented fracture; 2,959 m (9,706.9′). (F) Illite/smectite dolomitic mudstone micro-facies with partially cemented halite-filled fracture; 2,945 m (9,662.4′). (Q) Quartz, (C) Calcite, (D) Dolomite, (F) Feldspar, (Il/S) Illite/smectite, (H) Halite, (P) Pyrite, (Om) Organic matter, and (Φ_{om}) Organic matter porosity.

(Rasmussen & Rasmussen, 2009; Whidden et al., 2014; Jagniecki et al., 2019). The Cane Creek Shale has been subdivided into 3 zones noted by Jagniecki et al. (2019) and McCormack et al. (2023) (Figure 3). The A zone has been characterized by abundant anhydrite-dolomite with low sandstone and siltstone representing anoxic-saline conditions. Jagniecki et al. (2019) reported precipitated anhydrite, paleo-redox proxies V/(V+Ni), V/Cr, Ni/Co, Mo concentrations, pyrite, and lack of burrows and bioclasts in the A zone supporting a dysoxic/anoxic water column and pore waters. The B zone has been characterized by abundant very fine-grained sandstone and siltstone, generally lacking anhydrite, minor dolomite, high calcite, and organic-rich mudstone beds representing oxic-fresh conditions (Jagniecki et al., 2019). The C zone is characterized by abundant fine-grained sandstone and siltstone, dolomitic, organic-rich mudstone beds, gypsum, and anhydrite representing a transition from brine-saturated waters to fresher waters in mixed oxic-anoxic conditions (Jagniecki et al., 2019). Laminated microcrystalline anhydrite likely precipitated at the air-water interface and settled to the bottom where nodular anhydrite formed displacively within the sediment matrix creating soft sediment deformation from outward growth. Anhydrite in the Cane Creek Shale likely originated from gypsum.

Dolomite is commonly observed as fine crystalline, non-planar to planar texture in the mudstone micro-facies interpreted to have precipitated at the sediment interface syn-depositionally (Rasmussen & Rasmussen, 2009; Whidden et al., 2014). These euhedral dolomitic crystals with sulfide (pyrite) cements are formed during hyper-saline, near-surface, low-temperature environments associated with evaporitic sediments in the early stages of diagenesis with methagenesis and microbial sulfate reduction (Raiswell, 1982; Gregg & Sibley, 1984; Coleman, 1985; Curtis & Coleman, 1986; Gregg & Shelton, 1990; Haeri-Ardakani et al., 2013; Macquaker et al., 2014). These hyper-saline environments coincide with a supratidal depositional environment with sabkha evaporitic settings and a bacterial reducing environment during a marine transgression and evaporation cyclic sea-level fluctuations (Jagniecki et al., 2019). These fining upward deposits represent commonly occurring marine inundation with an early carbonate and incomplete dolomite cementation overlain by evaporites indicating a desiccating sabkha environment. Similar modern-day sabkha analog environments include the sabkhas of Abu Dhabi, Persian Gulf, which is characterized by penecontemporaneous dolomite and carbonate with distinct laminae and chicken-wire anhydrite (Warren & Kendall, 1985; Court et al., 2017) similar to described mudstone micro-facies.

Thick siliciclastic deposits, quartz-rich, very fine sandstone micro-facies, previously described as fine-grained sandy siltstone, dominate the middle stratigraphic trend, previously interpreted as lowstand deposits (Figure 3) (Goldhammer et al., 1991; Rasmussen & Rasmussen, 2009; Jagniecki et al., 2019). These micro-facies are moderately to well sorted, subangular to subrounded, mostly siliciclastic grains indicating some transport. Siliciclastic grains were likely river-fed and transported into the Paradox Basin from the Uncompahgre uplift. The moderate to well-sorted grains in this micro-facies indicate possible wave reworking by tidal influence in shallow marine waters in subtidal, intertidal, and supratidal zones once in the basin depocenter (Figure 5) (Jagniecki et al., 2019). Moderate to well-sorted siliciclastic grains with carbonate cement (Figure 5) and poorly sorted to moderate, organic-rich, dolomitic mudstones (Figure 7), all represent shallow-marine to tidal environments. Silt-sized siliciclastic grains in finer micro-facies are likely eolian transported grains reworked with fluvial and wave influence, previously recognized in the southwest basin margin during highstand marine transgression (Rasmussen & Rasmussen, 2009). Silt-sized, aeolian loess has been identified from the Lower Permian/Upper Pennsylvanian (i.e., proximal Cutler Formation) and Lower Pennsylvanian (i.e., Molas Formation) from western Pangea and the surrounding Ancestral Rocky Mountains region of western North America (Evans & Reed, 2007; Soreghan et al., 2008). Laminated dolomitic mudstone with moderately sorted, very fine-grained sandstone packages have been interpreted as aeolian or suspended origin settling from Leonardian shelf deposits in the Permian Basin (Saller et al., 1989; Nicot et al., 2023).

5.2. Diagenesis implications on reservoir quality

Depositional controls such as mineralogical composition, matrix, cements, grain sorting, grain size, and diagenetic physical and chemical controls influence overall reservoir quality and have implications on porosity and permeability (Burley et al., 1985; Lazar et al., 2015; Egenhoff et al., 2019; Quandt et al., 2022). Detrital mineralogy of coeval siliciclastic and carbonate deposition provides an initial mineralogical composition that can be affected by diagenetic controls following deposition (Macquaker et al., 2007, 2014; Taylor & Macquaker, 2014; Fishman et al., 2015). Though the core is located at the northern end of the basin and may not be exactly representative of the basin, the entire Cane Creek interval was sampled, measured, and analyzed to recognize the majority of the diagenetic effects.

The Early (eogenesis) stage coincides with deposition and initial burial, Middle (mesogenesis) stage with continued burial and deepest basin burial, and Late (telogenesis) stage with the uplift of the basin, all of which include components that affect reservoir quality (Choquette & Pray, 1970; Burley et al., 1985; Moore, 1989). The relative timing of events with a thermal burial and hydrocarbon generation model of the Cane Creek Shale in the Moab, UT area (Nuccio & Condon, 1996) highlights major diagenetic timing events relative to tectonic events in the Paradox Basin (Figure 11B).

After the initial deposition of the Cane Creek Shale, compaction and cementation lead to a reduction in sediment volume and porosity resulting in decreased reservoir quality (Houseknecht, 1987; Quandt et al., 2022). Early authigenic cements have the potential to dissolve and allow secondary precipitates to infill the pore space. Siliciclastic-rich samples are susceptible to minor sheltered porosity by cements prior to compaction (Macquaker et al., 2014; Taylor & Macquaker, 2014). From SEM and petrography, minor concave-convex and sutured gain contacts in the Cane Creek Shale provide evidence of moderate compaction. Compaction is evident in siliciclastic and carbonate-dolomitic micro-facies observed as grain-to-grain contacts and fractured grains. Compaction has been directly related to porosity reduction in coarser sandstone systems as well as siliceous mudrocks (Makowitz et al., 2006; Milliken & Olson, 2017). High compaction will reduce available surface area and can inhibit authigenic mineral precipitation. Quartz overgrowths are minor and ubiquitously in siliciclastic-rich micro-facies, linked to the low degree of pressure solution as the Cane Creek Shale did not reach optimal temperatures in the Early stage (>100 °C (212 °F)) for quartz nucleation (Giles et al., 1992; Huggett, 1996; Taylor et al., 2010; Milliken & Olson, 2017). Furthermore, due to abundant authigenic clay cements, quartz overgrowth nucleation was hindered by a lack of available surface hindered by detrital or authigenic clays.

The primary controls on reservoir quality in the Cane Creek Shale are authigenic cements, specifically an Early stage dolomite, carbonate, illite/smectite clay domains and cement, and Middle stage anhydrite cement and minor quartz cement. Original displaced depositional clay domains can reduce porosity and permeability along with authigenic cementation. Permeability reduction has been modeled directly to the growth of authigenic abundance and its associated surface area (Howard, 1992). Enhanced surface area lends to greater pore water fluid fluxes in mudstone micro-facies aided by compaction and chemical changes (i.e., dissolution and precipitation) at greater depths (Bjørlykke, 1999). Dolomite and illite/smectite authigenic clay cements have opposing effects on reservoir quality related to porosity and permeability. Illite/smectite authigenic clay cements reduce porosity and permeability, whereas Early stage dolomite and carbonate grains can preserve porosity and permeability, even after compaction, by preserving early pore space.

Siliciclastic (sandstone to siltstone) micro-facies reservoir quality exhibits optimal porosity and permeability but can be negatively impacted by illite/smectite authigenic clays, dependent on textural maturity, and halite and anhydrite cements. Halite-dominated deposits eliminate pore space within the first few tens of meters of burial and therefore are not capable of storing large volumes of brine in pore spaces (Casas & Lowenstein, 1989; Warren, 2010). Surface-formed brines must flow to more porous and permeable sediments. The coarsest micro-facies (quartz-rich, very fine sandstone and calcareous, silty sandstone) show moderate porosities with moderate to high permeabilities (Figure 10). Sandstone micro-facies are the micro-facies with abundant quartz and feldspars grains. Feldspars are more likely to experience dissolution and precipitate authigenic quartz (i.e., minor quartz overgrowths) and illite/smectite clay cements. Authigenic illite/smectite is capable of reducing effective pore space by cement lining or infill (Pittman et al., 1992; Quandt et al., 2022). Siliciclastic illite/smectite clay domains are capable of encasing grains and reducing porosity (Schieber et al., 2016). Illite/smectite authigenic clay cement is highly variable and aided by the abundance of feldspar grains and degree of dissolution that contribute silica and aluminum into solution. Because of variable illite/smectite cement, the sandstone micro-facies of the Cane Creek Shale show a moderate range in porosity and permeability values. Il/S dolomitic mudstone micro-facies shows the highest porosity and permeabilities of the dataset. However, these high values are inferred as induced fracture porosity with enhanced permeabilities and thus not representative of the Cane Creek Shale's true in-situ porosity and permeability.

Dolomitic and carbonate grain sorting and lack of illite/smectite authigenic cements positively impact carbonate and dolomitic-rich micro-facies (i.e., mudstone micro-facies) reservoir quality. Mudstone micro-facies lack high siliciclastic content and therefore do not have the high abundance of illite/smectite cement observed in sandstone to siltstone micro-facies, although authigenic clays are still present in minor abundance. Carbonate and dolomitic micro-facies (calcareous, silty mudstone and calcareous, dolomitic mudstone) show a slightly higher range in porosity values and permeabilities than sandstone micro-facies (Figure 10). Compaction plays a role in reducing porosity in all micro-facies but due to the early diagenetic formation of a brittle carbonate and dolomite grains found in siltstone and mudstone micro-facies preserves primary intergranular porosity. Lack of illite/smectite cement in dolomitic mudstones does not hinder porosity and allows for porosity and permeability values comparable to or slightly higher than in sandstone micro-facies. Secondary porosity from the dissolution of carbonate and dolomite grains can produce additional porosity in the Cane Creek Shale. In general, secondary porosity in other petrographic and modeling studies has been interpreted to be negligible to the overall reservoir quality (Taylor et al., 2010).

Anhydritic-dolomudstone micro-facies reservoir quality is negatively impacted by evaporitic anhydrite cements usually found as nodules or pore-filling cements. These facies lack siliciclastic input and are characterized by low to high authigenic anhydrite cement. Anhydritic-dolomudstone micro-facies shows the lowest porosity values and low to high range in permeabilities (Figure 10). In general, porosity and permeability values are low with a few anomalously high permeability values. These high permeability values are likely associated with partial

halite-cemented fractures and lack of matrix permeability due to high anhydrite cementation.

6. Conclusions

A high-resolution analysis using petrography and SEM analysis with EDS composite elemental maps was completed on the previously understudied fine-grained Cane Creek Shale of the Paradox Basin in southeastern Utah. This study describes diagenetic controls influenced by original depositional mineralogy in a fine-grained, evaporitic, sabkha environment. Identified critical compositional heterogeneities in the fine-grained deposits directly affect reservoir quality and the producibility for hydrocarbon exploration potential in the Cane Creek Shale. Petrographic micro-facies characterization also has applications in energy development that can be applied to hydrocarbon and geothermal resources, carbon capture, and hydrogen storage. This study lends to a growing number of studies and literature on poorly understood fine-grained deposits, including mudstones and quartz-rich, very fine sandstones. A greater understanding of diagenetic mineralogy and its effects on porosity and permeability development helps to better understand reservoir quality and potential seals in fine-grained deposits that contain evaporites.

Twelve micro-facies, grouped into three main micro-facies types: sandstone to siltstone, mudstone, and evaporitic micro-facies were identified from the Zephyr Energy State 16-2 research well. A detailed porosity and mineralogy micro-facies analysis was completed of a cored interval from the Pennsylvanian Cane Creek Shale. Dominant types of cements include varying degrees of illite/smectite, calcite, halite, and a lesser degree of anhydrite, dolomite, and quartz overgrowths.

Micro-facies mineralogy is the primary control on identified pore types for the Cane Creek Shale. Sandstone to siltstone micro-facies show a range in ideal measured porosity and permeability values characterized by primarily intergranular porosity with minor dissolution intragranular porosity. Variability in porosity values, characterized by intergranular porosity in sandstone to siltstone micro-facies, is dependent on the degree of illite/smectite domains or authigenic cements (i.e., authigenic illite/smectite, quartz overgrowths, halite, dolomite, etc.) and is primarily controlled by siliciclastic composition. Quartz and feldspar dissolution can lead to variable abundance of authigenic illite/smectite in sandstone micro-facies. This in turn can significantly reduce the available storage capacity by reducing porosity by authigenic cementation.

Dolomitic mudstone micro-facies show low porosity and permeability values characterized by intergranular porosity with minor organic matter and clay domain nanopores. Early brittle carbonate and dolomite grain sorting preserves porosity in dolomitic siltstone and mudstone micro-facies. Carbonate grain sorting and minor interconnected pore networks control low porosity and permeability. Anomalously high porosity and permeability values from some mudstone micro-facies are likely associated with delamination associated with drilling, exhumation, and sample prep damage, rather than in-situ porosity and permeability.

A paragenetic sequence of the relative timing of authigenic cementation and events was developed for the Cane Creek Shale, highlighting early, middle, to late stage short-term to long-lived diagenetic events affecting reservoir quality. Early-stage grain compaction, early carbonate cements, feldspar dissolution and authigenic cementation (i.e., pyrite and illite/smectite) are associated with the long-lived slow burial of the basin, limiting porosity and permeability. A Middle stage event of authigenic cementation is defined by carbonate precipitation and minimal quartz overgrowth stage. Finally, a Late stage timing of events includes anhydrite cementation, fracturing, and delamination associated with basin uplift and mobilized halite and precipitation.

Acknowledgments

This work was funded by the U.S. Department of Energy to the University of Utah (PI, Dr. Brian McPherson), project titled "Improving Production in the Emerging Paradox Oil Play" (DE-FE0031775). This work was supported by the U.S. Department of Energy award #DE-FOA-0001990. We are also grateful to Zephyr Energy, LLC, for financial support, technical operations, collection, and collaboration of the research State 16-2 core. The authors would like to thank Cari Johnson, professor at the University of Utah, Jesus Salazar, senior petrophysicist at Marathon Oil Corporation, and Joe Macquaker, geoscientist at ExxonMobil for their contributions to an early draft of the manuscript. Many thanks to Miranda Clow from the University of Utah for imaging and documenting traditional petrography micrographs. Thank you to Paulo Perez, Van Devener, and the faculty at the Biotechnology Nanofab lab at the University of Utah for scanning electron microscopy technical support. Fieldwork and subsequence interpretation/analysis at the University of Utah was conducted within the traditional and ancestral homeland of the Shoshone, Paiute, Goshute, Pueblo, and Nuutsui (Ute) Tribes (https://president.utah.edu/indigenous-land-acknowledgment/).

Authors contribution

Data acquisition: R.I. Ochoa, L. Birgenheier, E. Jagniecki, M.D. Vanden Berg. Analysis and Interpretation: R.I. Ochoa. Additional interpretations, writing, and revision: L. Birgenheier, E. Jagniecki, M.D. Vanden Berg. All authors have read and agreed to the published version of the manuscript.

Data availability

The data for the manuscript, figures, and tables are available upon author's request.

Conflict of interest

The authors declare no conflict of interest.

References

Awwiller, D. N. (1993). Illite/smectite formation and potassium mass transfer during burial diagenesis of mudrocks; a study from the Texas Gulf Coast Paleocene-Eocene. Journal of Sedimentary Petrology, 63(3), 501–512. https://doi.org/10.1306/D4267B3B-2B26-11D7-8648000102C1865D

Barbeau, D. L. (2003). A flexural model for the Paradox Basin: Implications for the tectonics of the Ancestral Rocky Mountains. Basin Research, 15(1), 97–115. https://doi.org/10.1046/j.1365-2117.2003.00194.x

Berner, R. A. (1970). Sedimentary pyrite formation. American Journal of Science, 268(1), 1–23. https://doi.org/10.2475/ajs.268.1.1

Bjørlykke, K. (1999). Principal aspects of compaction and fluid flow in mudstones. Geological Society Special Publication, 158, 73–78. https://doi.org/10.1144/GSL.SP.1999.158.01.06

Blair, T. C., & McPherson, J. G. (1999). Grain-size and textural classification of coarse sedimentary particles. Journal of Sedimentary Research, 69(1), 6–19. https://doi.org/10.2110/jsr.69.6

Burley, S. D., Kantorowicz, J. D., & Waugh, B. (1985). Clastic Diagenesis. Geological Society of London Special Publication, (1979), 189–226. https://doi.org/10.1144/GSL.SP.1985.018.01.10

Busch, B., Adelmann, D., Herrmann, R., & Hilgers, C. (2022). Controls on compactional behavior and reservoir quality in a Triassic Buntsandstein reservoir, Upper Rhine Graben, SW Germany. Marine and Petroleum Geology, 136, 105437. https://doi.org/10.1016/j.marpetgeo.2021.105437

Casas, E., & Lowenstein, T. K. (1989). Diagenesis of saline pan halite: Comparisions of petrographic features of modern, Quaternary and Permian halites. Journal of Sedimentary Petrology, 59(5), 724–739. https://doi.org/10.1306/212F905C-2B24-11D7-8648000102C1865D

Choquette, P. W., & Pray, L. C. (1970). Geologic Nomenclature and Classification of Porosity in Sedimentary Carbonates. American Association of Petroleum Geologists Bulletin, 54(2), 207–250. https://doi.org/10.1306/5d25c98b-16c1-11d7-8645000102c1865d

Coleman, M. L. (1985). Geochemistry of Diagenetic Non-Silicate Minerals Kinetic Considerations. Philosophical Transactions of the Royal Society of London, A315(1531), 39–56. https://doi.org/10.1098/rsta.1985.0028

Court, W. M., Paul, A., & Lokier, S. W. (2017). The preservation potential of environmentally diagnostic sedimentary structures from a coastal sabkha. Marine Geology, 386, 1–18. https://doi.org/10.1016/j.margeo.2017.02.003

Curtis, C. D., & Coleman, M. L. (1986). Controls on the precipitation of early diagenetic calcite, dolomite and siderite concretions in complex depositional sequences. Roles of Organic Matter in Sediment Diagenesis (SP38), 23–33. https://doi.org/10.2110/pec.86.38.0023

Dean, W. E., & Stark, D. D. (1920). A convenient method for the determination of water in petroleum and other organic emulsions. The Journal of Industrial and Engineering Chemistry, 12(5), 486–490. https://doi.org/10.1021/ie50125a025

Dunham, R. J. (1962). Classification of carbonate rocks according to depositional textures. Classification of Carbonate Rocks--A Symposium, 108–121. https://doi.org/10.1306/M1357

Egenhoff, S. O., Fishman, N. S., Lowers, H. A., & Ahlberg, P. (2019). The complexity of mudstone diagenesis–some insight from the Tøyen Shale, Lower to Middle Ordovician, southern Sweden. Gff, 141(1), 54–67. https://doi.org/10.1080/11035897.2018.1525620

Evans, J. E., & Reed, J. M. (2007). Integrated loessite-paleokarst depositional system, early Pennsylvanian Molas Formation, Paradox Basin, southwestern Colorado, U.S.A. Sedimentary Geology, 195(3–4), 161–181. https://doi.org/10.1016/j.sedgeo.2006.07.010

Fielding, C. R. (2021). Late Palaeozoic cyclothems – A review of their stratigraphy and sedimentology. Earth-Science Reviews, 217, 103612. https://doi.org/10.1016/j.earscirev.2021.103612

Fishman, N. S., Egenhoff, S. O., Boehlke, A. R., & Lowers, H. A. (2015). Petrology and diagenetic history of the upper shale member of the late Devonian-early Mississippian Bakken Formation, Williston Basin, North Dakota. Special Paper of the Geological Society of America, 515, 125–151. https://doi.org/10.1130/2015.2515(07)

Folk, R. L. (1954). The distinction between grain size and mineral composition in sedimentary-rock nomenclature. The Journal of Geology, 62(4), 344–359. https://doi.org/10.1086/626171

Giles, M. R., Stevenson, S., Martin, S. V., Cannon, S. J. C., Hamilton, P. J., Marshall, J. D., & Samways, G. M. (1992). The reservoir properties and diagenesis of the Brent Group; a regional perspective. In A. C. Morton, R. S. Haszeldine, M. R. Giles, & S. Brown (Eds.), Geological Society Special Publications (pp. 289–328). Geological Society of London, London, United Kingdom. https://doi.org/10.1144/GSL.SP.1992.061.01.16

Goldhammer, R. K., Oswald, E. J., & Dunn, P. A. (1991). Hierarchy of stratigraphic forcing: Example from Middle Pennsylvanian shelf carbonates of the Paradox basin. Bulletin of the Kansas Geological Society, Vol. 233, pp. 361–413. http://www.kgs.ku.edu/Publications/Bulletins/233/Goldhammer/

Gregg, J. M., & Shelton, K. L. (1990). Dolomitization and dolomite neomorphism in the back reef facies of the Bonneterre and Davis formations (Cambrian), southeastern Missouri. Journal of Sedimentary Petrology, 60(4), 549–562. https://doi.org/10.1306/212F91E2-2B24-11D7-8648000102C1865D

Gregg, J. M., & Sibley, D. F. (1984). Epigenetic dolomitization and the origin of xenotopic dolomite texture. Journal of Sedimentary Petrology, 54(3), 908–931. https://doi.org/10.1306/212F8535-2B24-11D7-8648000102C1865D

Grove, K. W., Horgan, C. C., Flores, F. E., & Al., E. (1993). Bartlett Flat Big Flat (Kane Springs Unit). In B. G. Hill & S. R. Bereskin (Eds.), Oil and Gas Fields of Utah: 22. Utah, USA.

Haeri-Ardakani, O., Al-Aasm, I., Coniglio, M., & Samson, I. (2013). Diagenetic evolution and associated mineralization in Middle Devonian carbonates, southwestern Ontario, Canada. Bulletin of Canadian Petroleum Geology, 61(1), 41–58. https://doi.org/10.2113/gscpgbull.61.1.41

Hite, R. J. (1960). Stratigraphy of the saline facies of the southeastern Paradox Member of the Hermosa Formation of southeastern Utah and southwestern Colorado: Four Corners Geological Assocation. 3rd Annual Field Conference Guidebook, 86–89. https://doi.org/10.3133/ofr6070

Hite, R. J., Anders, D. E., & Ging, T. G. (1984). Organic-rich source rocks of the Pennsylvanian age in the Paradox Basin of Utah and Colorado. Hydrocarbon Source Rocks of the Greater

Rocky Mountain Region, 255–274. https://doi.org/10.1002/jps.2600680318

Hite, R. J., & Buckner, D. H. (1981). Stratigraphic correlations, facies concepts, and cyclicity in Pennsylvanian rocks of the Paradox Basin. In D. L. Wiegand (Ed.), Geology of the Paradox Basin Rocky Mountain Association of Geologists Field Conference (pp. 147–159).

Houseknecht, D. W. (1987). Assessing the relative importance of compaction processes and cementation to reduction of porosity in sandstones. American Association of Petroleum Geologists Bulletin, 71(6), 633–642. https://doi.org/10.1306/9488787f-1704-11d7-8645000102c1865d

Howard, J. J. (1992). Influence of Authigenic-Clay Minerals on Permeability. Origin, Diagenesis, and Petrophysics of Clay Minerals in Sandstones, (47), 257–264. https://doi.org/10.2110/pec.92.47.0257

Huggett, J. M. (1996). Aluminosilicate diagenesis in a Tertiary sandstone-mudrock sequence from Central North Sea, UK. Clay Minerals, (31), 523–536. https://doi.org/10.1180/claymin.1996.031.4.10

Jagniecki, E. A., Gall, R., Sitla, T. W., & Berg, M. Vanden. (2019). Geologic Characterization of the Northern Cane Creek Shale Play, Paradox Basin, Utah.

Jagniecki, E. A., Vanden Berg, M., Ochoa, R. I., & Birgenheier, L. P. (2022). Sedimentology and Reservoir Characterization of the Emerging Cane Creek Play, Paradox Formation, Northern Paradox Basin, Southeastern Utah. AAPG Rocky Mountain Section Meeting, Denver, CO, 24-27 July 2022.

Karner, S. L., Chester, J. S., Chester, F. M., Kronenberg, A. K., & Hajash, A. (2005). Laboratory deformation of granular quartz sand: Implications for the burial of clastic rocks. American Association of Petroleum Geologists Bulletin, 89(5), 603–625. https://doi.org/10.1306/12200404010

Lazar, O. R., Bohacs, K. M., Macquaker, J. H. S., Schieber, J., & Demko, T. M. (2015). Capturing Key Attributes of Fine-Grained Sedimentary Rocks In Outcrops, Cores, and Thin Sections: Nomenclature and Description Guidelines. Journal of Sedimentary Research, 85(3), 230–246. https://doi.org/10.2110/jsr.2015.11

Li, Z., & Schieber, J. (2020). Application of sequence stratigraphic concepts to the Upper Cretaceous Tununk Shale Member of the Mancos Shale Formation, south-central Utah: Parasequence styles in shelfal mudstone strata. Sedimentology, 67(1), 118–151. https://doi.org/10.1111/sed.12637

Löhr, S. C., Baruch, E. T., Hall, P. A., & Kennedy, M. J. (2015). Is organic pore development in gas shales influenced by the primary porosity and structure of thermally immature organic matter? Organic Geochemistry, 87, 119–132. https://doi.org/10.1016/j.orggeochem.2015.07.010

Loucks, R. G., Reed, R. M., Ruppel, S. C., & Hammes, U. (2012). Spectrum of pore types and networks in mudrocks and a descriptive classification for matrix-related mudrock pores. AAPG Bulletin, 96(6), 1071–1098. https://doi.org/10.1306/08171111061

Lucia, F. J. (1983). Petrophysical parameters estimated from visual descriptions of carbonate rocks: a field classification of carbonate pore space. Journal of Petroleum Technology, 35(3), 629–637. https://doi.org/10.2118/10073-PA

Lutz, S. J., Hickman, S., Davatzes, N., Zemach, E., Drakos, P., & Robertson-Tait, A. (2010). Rock mechanical testing in support of well stimulation activities at the Desert Peak geothermal field, Nevada. Transactions - Geothermal Resources Council, 34 1, 341–348.

Macquaker, J. H. S., Taylor, K. G., & Gawthorpe, R. L. (2007). High-resolution facies analyses of mudstones: Implications for paleoenvironmental and sequence stratigraphic interpretations of offshore ancient mud-dominated successions. Journal of Sedimentary Research, 77(4), 324–339. https://doi.org/10.2110/jsr.2007.029

Macquaker, J. H. S., Taylor, K. G., Keller, M., & Polya, D. (2014). Compositional controls on early diagenetic pathways in fine-grained sedimentary rocks: Implications for predicting unconventional reservoir attributes of mudstones. AAPG Bulletin, 98(3), 587–603. https://doi.org/10.1306/08201311176

Makowitz, A., Lander, R. H., & Milliken, K. L. (2006). Diagenetic modeling to assess the relative timing of quartz cementation and brittle grain processes during compaction. American Association of Petroleum Geologists Bulletin, 90(6), 873–885. https://doi.org/10.1306/12190505044

McCormack, K. L., McLennan, J. D., Jagniecki, E. A., & McPherson, B. J. (2023). Discrete Measurements of the Least Horizontal Principal Stress from Core Data: An Application of Viscoelastic Stress Relaxation. SPE Reservoir Evaluation & Engineering, 26, 827–841. https://doi.org/10.2118/214669-pa

Milliken, K. L., & Olson, T. (2017). Silica Diagenesis, Porosity Evolution, and Mechanical Behavior in Siliceous Mudstones, Mowry Shale (Cretaceous), Rocky Mountains, U.S.A. Journal of Sedimentary Research, 87, 366–387. https://doi.org/10.2110/jsr.2017.24

Milliken, K. L., Rudnicki, M., Awwiller, D. N., & Zhang, T. (2013). Organic matter-hosted pore system, Marcellus Formation (Devonian), Pennsylvania. AAPG Bulletin, 97(2), 177–200. https://doi.org/10.1306/07231212048

Moore, C. H. (1989). Carbonate diagenesis and porosity. Elsevier.

Nicot, J. P., Darvari, R., Smye, K. M., & Goodman, E. (2023). Geochemical insights from formation waters produced from Wolfcampian and Leonardian intervals of the Midland Basin, Texas, USA. Applied Geochemistry, 150, 105585. https://doi.org/10.1016/j.apgeochem.2023.105585

Nuccio, V. F., & Condon, S. M. (1996). Burial and Thermal History of the Paradox Basin, Utah and Colorado, and Petroleum Potential of the Middle Pennsylvanian Paradox Formation. In Geology and Resources of the Paradox Basin: Utah Geological Association Guidebook 25 (p. 18). https://doi.org/10.3133/b00O

Pittman, E. D., Larese, R. E., & Heald, M. T. (1992). Clay Coats: Occurrence and Relevance To Preservation of Porosity in Sandstones. In D. W. Houseknecht & E. D. Pittman (Eds.), Origin, Diagenesis, and Petrophysics of Clay Minerals in Sandstones (pp. 241–255). https://doi.org/10.2110/pec.92.47.0241

Quandt, D., Busch, B., Schmidt, C., & Hilgers, C. (2022). Diagenesis and controls on reservoir quality of Lower Triassic red bed sandstones (Buntsandstein) from a marginal basin facies, southwest Germany. Marine and Petroleum Geology, 142, 105744. https://doi.org/10.1016/j.marpetgeo.2022.105744

Raiswell, R. (1982). Pyrite texture, isotopic composition and the availability of iron. American Journal of Science, 82, 1244–1263. https://doi.org/10.2475/ajs.282.8.1244

Rasmussen, L., & Rasmussen, D. L. (2009). Burial History Analysis of the Pennsylvanian Petroleum System in the Deep Paradox Basin Fold and Fault Belt, Colorado and Utah. RMAG Special Publication, The Parado, 24–94.

Saller, A. H., Barton, J. W., & Barton, R. E. (1989). Slope sedimentation associated with a vertically building shelf, Bone Spring Formation, Mescalero Escarpe field, southeastern New Mexico.

Controls on Carbonate Platform and Basin Development, 275–288. https://doi.org/10.2110/pec.89.44.0275

Schieber, J., Lazar, R., Bohacs, K., Klimentidis, R., Dumitrescu, M., & Ottmann, J. (2016). An SEM study of porosity in the eagle ford shale of Texas-pore types and porosity distribution in a depositional and sequence-stratigraphic context. AAPG Memoir, 110, 167–186. https://doi.org/10.1306/13541961M1103589

Sondergeld, C. H., Newsham, K. E., Comisky, J. T., Rice, M. C., & Rai, C. S. (2010). Petrophysical Considerations in Evaluating and Producing Shale Gas Resources. SPE Unconventional Gas Conference. https://doi.org/10.2118/131768-MS

Soreghan, G. S., Soreghan, M. J., & Hamilton, M. A. (2008). Origin and significance of loess in late Paleozoic western Pangaea: A record of tropical cold? Palaeogeography, Palaeoclimatology, Palaeoecology, 268(3–4), 234–259. https://doi.org/10.1016/j.palaeo.2008.03.050

Soreghan, G. S., Soreghan, M. J., Sweet, D. E., & Moore, K. D. (2009). Hot Fan or Cold Outwash? Hypothesized Proglacial Deposition in the Upper Paleozoic Cutler Formation, Western Tropical Pangea. Journal of Sedimentary Research, 79, 495–522. https://doi.org/10.2110/jsr.2009.055

Stevenson, G. M., & Wray, L. L. (2009). History of Petroleum Exploration of Paleozoic Targets in the Paradox Basin. Rocky Mountain Association of Geologists, Special Publication, 1–23.

Stokes, W. L. (1986). Geology of Utah (sixth edit). Utah, USA: Utah Museum of Natural History.

Taylor, K. G., & Macquaker, J. H. S. (2000). Early diagenetic pyrite morphology in a mudstone-dominated succession: The Lower Jurassic Cleveland Ironstone Formation, eastern England. Sedimentary Geology, 131(1–2), 77–86. https://doi.org/10.1016/S0037-0738(00)00002-6

Taylor, K. G., & Macquaker, J. H. S. (2014). Diagenetic alterations in a silt- and clay-rich mudstone succession: an example from the Upper Cretaceous Mancos Shale of Utah, USA. Clay Minerals, 49(2), 213–227. https://doi.org/10.1180/claymin.2014.049.2.05

Taylor, T. R., Giles, M. R., Hathon, L. A., Diggs, T. N., Braunsdorf, N. R., Birbiglia, G. V., Kittridge, M. G., Macaulay, C. I., Espejo, I. S. (2010). Sandstone diagenesis and reservoir quality prediction: Models, myths, and reality. American Association of Petroleum Geologists Bulletin, 94(8), 1093–1132. https://doi.org/10.1306/04211009123

Trudgill, B. D. (2011). Evolution of salt structures in the northern Paradox Basin: controls on evaporite deposition, salt wall growth and supra-salt stratigraphic architecture. Basin Research, 23(2), 208–238. https://doi.org/10.1111/j.1365-2117.2010.00478.x

Udden, J. A. (1914). Mechanical Composition of Clastic Sediments. Geological Society of America Bulletin, 25, 655–744. https://doi.org/doi.org/10.1130/GSAB-25-655

Warren, J. K. (2010). Evaporites through time: Tectonic, climatic and eustatic controls in marine and nonmarine deposits. Earth-Science Reviews, 98(3–4), 217–268. https://doi.org/10.1016/j.earscirev.2009.11.004

Warren, J. K., & Kendall, C. G. C. (1985). Comparison of Sequences Formed in Marine Sabkha and Salina Settings C Modern and Ancient. AAPG Bulletin, 69, 1013–1023. https://doi.org/http://dx.doi.org/10.1306/AD462B46-16F7-11D7-8645000102C1865D

Whidden, K. J., Anna, L. O., Pearson, K. M., & Lillis, P. G. (2012). Assessment of Undiscovered Oil and Gas Resources in the Paradox Basin Province, Utah, Colorado, New Mexico, and Arizona. U.S. Geological Survey Fact Sheet 2012-3031, 4.

Whidden, K. J., Lillis, P. G., Anna, L. O., Pearson, K. M., & Dubiel, R. F. (2014). Geology and Total Petroleum Systems of the Paradox Basin, Utah, Colorado, New Mexico, and Arizona. The Mountain Geologist, 51(2), 119–138.

Yau, Y.-C., Peacor, D. R., & Mcdowell, S. D. (1987). Smectite-to-illite reactions in salton sea shales: a transmission and analytical electron microscopy study. Journal of Sedimentary Petrology, 57(2), 335–342. https://doi.org/10.1306/212F8B20-2B24-11D7-8648000102C1865D

How to cite: Ochoa, R., Birgenheier, L., Jagniecki, E., & Michael. (2024). Micro-facies characterization of the Cane Creek Shale, Paradox Basin, Utah: implications of diagenetic controls on reservoir quality. Sedimentologika, 2(2). 1-28. https://doi.org/10.57035/journals/sdk.2024.e22.1278